INSTITUTE OF PHYSICS PUBLISHING WAVES IN RANDOM MEDIA

Waves Random Media **13** (2003) 27–58 PII: S0959-7174(03)38502-7

Shadowing function with single reflection from anisotropic Gaussian rough surface. Application to Gaussian, Lorentzian and sea correlations

C Bourlier[1] **and G Berginc**[2]

[1] IRCCyN : UMR n° 6597 CNRS, Division SETRA Ecole Polytechnique de l'Université de Nantes—IRESTE, Rue Christian Pauc, La Chantrerie, BP 60601, 44306 NANTES Cedex 3, France
[2] DS/DFO, THALES Optronique, Rue Guynemer, BP 55, 78283 Guyancourt Cedex, France

E-mail: christophe.bourlier@polytech.univ-nantes.fr

Received 17 June 2002, in final form 24 September 2002
Published 6 November 2002
Online at stacks.iop.org/WRM/13/27

Abstract

In this paper, the monostatic (transmitter and receiver are located at the same place) and bistatic (transmitter and receiver are distinct) statistical shadowing functions from an anisotropic two-dimensional randomly rough surface are presented. This parameter is especially important in the case of grazing angles for computing the bistatic scattering coefficient in optical and microwave frequencies. The objective of this paper is to extend the previous work (Bourlier C, Berginc G and Saillard J 2002 *Waves Random Media* **12** 145–74), valid for a one-dimensional surface, to a two-dimensional anistropic surface by considering a joint Gaussian process of surface slopes and heights separating two points of the surface. The monostatic average (statistical shadowing function average over the statistical variables) shadowing function is then performed in polar coordinates with respect to the incidence angle, the azimuthal direction and the surface height two-dimensional autocorrelation function. In addition, for a bistatic configuration, it depends on the incidence angle and azimuthal direction of the receiver. For Gaussian and Lorentzian correlation profiles and practically important power-type spectra such as the Pierson–Moskowitz sea roughness spectrum, the numerical solution, obtained from generating the surface Gaussian elevations (Monte Carlo method), is compared with the uncorrelated and correlated models. The results show that the correlation underestimates the shadow slightly, whereas the uncorrelated results weakly overpredict the shadow and are close to the numerical solution.

1. Introduction

The problem of electromagnetic wave scattering from a randomly rough surface has been widely studied because of its relevance in the fields of telecommunications and remote sensing. To obtain semi-analytical models of the scattering coefficient or emissivity for microwave [1–11] and optical frequencies [12–14], assumptions are used on the surface roughness. We can quote the Kirchhoff approach, the small-perturbation model, the phase perturbation model, the full wave method (see [11]) and the small-slope approximation (see [8]). The two-scale model, which is a combination of the Kirchhoff and small-perturbation models, fails when the illumination grazing angle is small [1]. One reason for this failure is that the theoretical models do not directly account for the effects of the surface self-shadowing that occurs under these illumination conditions. Attempts have been made to extend the scattering models to smaller grazing angles by introducing shadowing functions that reduce the predicted scattering. The unshadowed scattering coefficient [1–7] is then multiplied by the average shadowing function integrated over the surface heights and slopes. As shown by Sancer [15], this procedure is valid for the geometrical optics approximation (solution of the Kirchhoff integral for the high-frequency limit). On the other hand [16, 17], with Kirchhoff's approximation, since the scattered field depends on the statistical variables, the statistical shadowing function has to account for the unshadowed scattering field to calculate the shadowed scattering cross section.

The problem of wave scattering by a rough surface in the presence of shadowing was first considered analytically in [18] and chapter 7 of [2] by means of the theory of random function overshoots developed in [19]. The statistical (this means that the average over the surface slopes and heights is not performed) shadowing function, defined as the ratio of the illuminated surface to the total area, is then expressed from an infinite series by Rice [2, 20, 21]. The shadowing effect with single reflection was rediscovered later with the Wagner [22], Smith [23, 24] and Beckman [25] formulations which approximate Rice's infinite series. Wagner and Beckman retain only the first term of the series, whereas Smith uses the Wagner approach by introducing a normalization function. For monostatic (transmitter and receiver located at the same place) and bistatic (transmitter and receiver are distinct) configurations, these authors assume a one-dimensional Gaussian surface where the correlation between the surface heights and slopes is omitted, meaning that the statistical shadowing function is independent of the surface height autocorrelation function. Recently, for a one-dimensional surface with a correlated Gaussian process of the surface heights and slopes, Bourlier *et al* [26, 27] show that the correlation can be neglected. Moreover, comparisons with numerical results computed from [28] show the Smith approach is more accurate than Wagner's. In [29], the shadowing effect is extended to a two-dimensional anisotropic surface for any uncorrelated process.

For monostatic and bistatic configurations, the objective of this paper is to extend the one-dimensional results to a two-dimensional anisotropic surface roughness in order to quantify the correlation effect on a Gaussian process. Firstly, for a monostatic configuration, the uncorrelated and correlated statistical shadowing functions are derived and compared with the exact numerical shadowing function computed from the algorithm developed by Brokelman and Hagfors [28]. The generation of surface heights, required for the numerical solution, cannot be treated as for the one-dimensional case. Indeed, to have a good representation of the surface statistics such as the surface height autocorrelation function and the height distribution, an important number of surface samples is required. For example, with a one-dimensional surface, the sample number is 100 000, which implies that with a two-dimensional surface the surface size could be $100\,000 \times 100\,000$, which requires a lot of memory. To overcome this problem, the surface is generated [30] with respect to the azimuthal direction ϕ which is similar to making a cross section of the two-dimensional surface according to ϕ. The advantage of

this method is to transform a two-dimensional problem to a one-dimensional problem along ϕ. The same method is used for the analytical calculations of the statistical shadowing function expressed in spherical coordinates.

The plan of this paper is defined as follows. Section 2 summarizes the results obtained for a one-dimensional surface since they are required from a two-dimensional configuration. In section 3, the statistical monostatic and bistatic shadowing functions are extended to a two-dimensional surface with the help of the one-dimensional formulation. Simulations are also presented for Gaussian and Lorentzian surface height autocorrelation functions and a sea surface spectrum. The study of the bistatic configuration leads to the case where the transmitter and the receiver are located in the same plane, and the second case, when they are in different planes where the correlation between the observed surface slopes at the same point is then accounted for, unlike [29]. In the last section, we give concluding remarks.

2. One-dimensional shadowing function

For a one-dimensional random surface [2, 20, 21], we give the rigorous expression of the statistical monostatic shadowing function equal to Rice's infinite series of integrals. For any uncorrelated process, the statistical and average shadowing functions can then be computed analytically [26]. Nevertheless, for an uncorrelated Gaussian process, the model has no physical meaning at grazing incidence angles. Moreover, when the correlation is introduced, the problem becomes very complicated and is not tractable analytically.

Therefore, the Wagner approach [22] which keeps only the first term of Rice's series, and the Smith [23, 24] formulation, which uses Wagner's approach with the introduction of the normalization function, are used for estimating the shadowing effect. Comparing both these models with the exact numerical solution, from a correlated Gaussian process with Gaussian and Lorentzian surface height autocorrelation functions, Bourlier *et al* [26] show that the Smith results are more accurate than Wagner's solution, and the correlation can be neglected. When the correlation is omitted, the shadowing effect is independent of the surface height autocorrelation function. The exact solution is computed by generating numerically the surface heights and slopes and applying the algorithm of Brokelman and Hagfors [28] summarized in figure 4 of [26]. The extension of the Smith formulation to a one-dimensional bistatic configuration leads to the same conclusion. Therefore, for a one-dimensional surface, the Smith formulation is the more accurate and it is used as a starting point to perform the shadowing effect.

In this section, the Smith formulation is summarized for monostatic and bistatic configurations with and without correlation. As will be shown in the next section, this reminder is required since the one-dimensional approach is used for a two-dimensional surface.

2.1. Monostatic shadowing function for an uncorrelated Gaussian process

For an observation length L_0, the statistical monostatic shadowing function $S(\theta, F, L_0)$ [22–24] is equal to the probability that the point $F(\xi_0, \gamma_0)$ on a random rough surface, of given height ξ_0 above the mean plane and with local slope $\gamma_0 = \partial\xi_0/\partial l$, is illuminated as the surface is crossed by an incident beam from incidence angle θ (figure 1)

$$S(\mu, F, L_0) = \Upsilon(\mu - \gamma_0) \exp\left[- \int_0^{L_0} g(\mu, F, l)\, \mathrm{d}l \right] \tag{1}$$

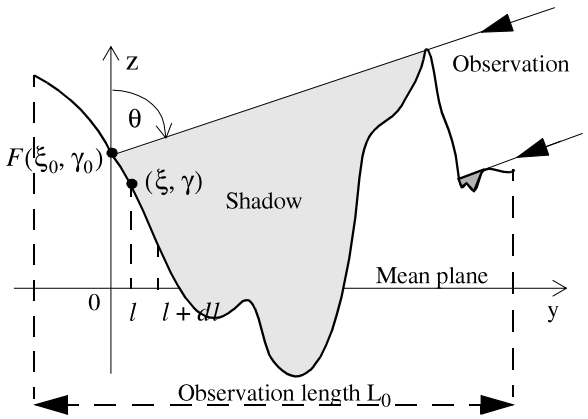

Figure 1. Monostatic shadowing function.

with

$$\Upsilon(\mu - \gamma_0) = \begin{cases} 0 & \text{if } \gamma_0 \geqslant \mu \\ 1 & \text{if } \gamma_0 < \mu \end{cases}, \text{ and } \mu = \cot\theta. \tag{1a}$$

$g(\mu, F, l)\,\mathrm{d}l$ is the conditional probability that the ray of slope $\mu = \cot\theta$ (θ denotes the incidence angle) intersects the surface in the interval $[l; l + \mathrm{d}l]$ and with the knowledge that the ray does not cross the surface in the interval $[0; l]$. Υ is the Heaviside function which carries a restriction on the surface slopes.

With the Smith formulation $g(\mu, F, l)$ is defined as follows:

$$g(\mu, F, l) = \frac{\int_{\mu}^{\infty}(\gamma - \mu)\,p(\xi, \gamma|\xi_0, \gamma_0; l)\,\mathrm{d}\gamma}{\int_{-\infty}^{\infty}\int_{-\infty}^{\xi_0+\mu l} p(\xi; \gamma|\xi_0, \gamma_0; l)\,\mathrm{d}\xi\,\mathrm{d}\gamma}, \tag{2}$$

with

$$\xi = \xi_0 + \mu l. \tag{2a}$$

In (2), $p(\xi, \gamma|\xi_0, \gamma_0; l)$ denotes the joint conditional probability over the surface heights $\{\xi_0, \xi\}$ and slopes $\{\gamma_0, \gamma\}$ separating two surface points. Substituting (2) into (1), for an arbitrary uncorrelated process, Bourlier *et al* ((12) and (12 *b*) of [26]) show that the statistical monostatic shadowing function is

$$S(\mu, F, L_0) = \Upsilon(\mu - \gamma_0)\left[\frac{P(\xi_0) - P(-\infty)}{P(\xi_0 + \mu L_0) - P(-\infty)}\right]^{\Lambda}, \tag{3}$$

where

$$\Lambda = \frac{1}{\mu}\int_{\mu}^{\infty}(\gamma - \mu)\,p(\gamma)\,\mathrm{d}\gamma, \qquad \text{and} \qquad P = \int p(\xi)\,\mathrm{d}\xi. \tag{3a}$$

The uncorrelated Gaussian process states

$$p(\xi)\,p(\gamma) = \frac{1}{2\pi\sigma\omega}\exp\left(-\frac{\xi^2}{2\omega^2} - \frac{\gamma^2}{2\sigma^2}\right), \tag{4}$$

where $\{\omega^2, \sigma^2\}$ denote the surface height and slope variances, respectively. Substituting (4) into (3) and (3*a*), $S(\mu, F, L_0)$ becomes

$$S(\mu, F, L_0) = \Upsilon(\mu - \gamma_0)\left[\frac{1 - \frac{1}{2}\mathrm{erfc}(\frac{\xi_0}{\sqrt{2}\omega})}{1 - \frac{1}{2}\mathrm{erfc}(\frac{\xi_0+\mu L_0}{\sqrt{2}\omega})}\right]^{\Lambda(\nu)}, \tag{5}$$

with

$$\Lambda(\nu) = \frac{\exp(-\nu^2) - \nu\sqrt{\pi}\,\mathrm{erfc}(\nu)}{2\nu\sqrt{\pi}}, \qquad \nu = \frac{\mu}{\sqrt{2}\sigma} = \frac{\cot\theta}{\sqrt{2}\sigma}, \tag{5a}$$

where erfc denotes the complementary error function. The Gaussian process with shadow becomes then $p(\xi_0, \gamma_0)S(\mu, F, L_0)$ where $p(\xi_0, \gamma_0)$ is the unshadowed process. This means that the shadowing effect carries a restriction over the surface slopes ($\gamma_0 \leqslant \mu = \cot\theta$ due to the $\Upsilon(\mu - \gamma_0)$ term) and modifies (term in brackets in (5)) the surface height distribution which becomes non-Gaussian (for an illustration see figure 2 of [26]).

The average shadowing function over the surface heights ξ_0 and slopes γ_0 is expressed as

$$S(\mu, L_0) = \int_{-\infty}^{\infty}\int_{-\infty}^{\infty} p(\xi_0, \gamma_0)S(\mu, F, L_0)\,\mathrm{d}\xi_0\,\mathrm{d}\gamma_0. \tag{6}$$

From the use of (5), for an infinite observation length ($L_0 \to \infty$), $S(\mu, L_0)$ is equal to

$$S(\nu, \infty) = [1 - \mathrm{erfc}(\nu)/2]/[1 + \Lambda(\nu)]. \tag{7}$$

For example, with a surface slope standard deviation $\sigma = 0.3$, incidence angles $\theta = \{80°, 85°\}$, we have $\nu = \{0.416, 0.206\}$ and $S = \{0.56, 0.32\}$ which is a decreasing function of θ, since the shadowing function is defined as the ratio of illuminated surface to the total area.

2.2. Monostatic shadowing function for a correlated Gaussian process

For a surface height $\{\xi, \xi_0\}$ and slope $\{\gamma, \gamma_0\}$ joint Gaussian process, $p(\xi, \gamma|\xi_0, \gamma_0; l)$ is expressed as (appendix 3 of [31])

$$p(\xi, \gamma|\xi_0, \gamma_0; l) = \frac{\sigma\omega}{2\pi\sqrt{|[C]|}}\exp\left[-\frac{C_{i11}(\xi_0^2 + \xi^2) + C_{i33}(\gamma_0^2 + \gamma^2)}{2|[C]|} + \frac{\xi_0^2}{2\omega^2} + \frac{\gamma_0^2}{2\sigma^2} - \frac{2C_{i12}\xi_0\xi + 2C_{i34}\gamma_0\gamma + 2C_{i13}(\xi_0\gamma_0 - \xi\gamma) + 2C_{i14}(\xi_0\gamma - \xi\gamma_0)}{2|[C]|}\right], \tag{8}$$

with

$$\begin{aligned} C_{i11} &= \omega^2(\sigma^4 - R_2^2) - R_1^2\sigma^2 & C_{i14} &= R_1(R_1^2 - R_0R_2 - \omega^2\sigma^2) \\ C_{i12} &= R_0(R_2^2 - \sigma^4) - R_1^2R_2 & C_{i33} &= \sigma^2(\omega^4 - R_0^2) - R_1^2\omega^2 \\ C_{i13} &= -R_1(R_0\sigma^2 + \omega^2R_2) & C_{i34} &= R_2(\omega^4 - R_0^2) + R_1^2R_0 \\ |[C]| &= (C_{i33}^2 - C_{i34}^2)/(\omega^4 - R_0^2) \end{aligned} \tag{8a}$$

where $R_0(l)$ is the height autocorrelation function, assumed even and derivable at the origin, and $\{R_1(l), R_2(l)\}$ are its first and second derivatives according to l. The surface height variance ω^2 is equal to $R_0(0)$ and the surface slope variance σ^2 is $-R_2(0)$. $|[C]|$ is the determinant of the covariance matrix $[C]$. The first subscript i in C_{iij} denotes the elements of the inverse matrix $[C]$ defined as

$$[C] = \begin{bmatrix} \omega^2 & R_0(l) & 0 & R_1(l) \\ R_0(l) & \omega^2 & -R_1(l) & 0 \\ 0 & -R_1(l) & \sigma^2 & -R_2(l) \\ R_1(l) & 0 & -R_2(l) & \sigma^2 \end{bmatrix}. \tag{9}$$

If the correlation is neglected, then $[C]$ is diagonal, and (8) becomes (4). Substituting (8) into (2) and (1) Bourlier *et al* (section 3.1 of [26]) show that the statistical shadowing function

with correlation is

$$S(\nu, h_0, \zeta_0, y_0) = \begin{cases} \Upsilon(\nu - \zeta_0) \exp\left[-L_c \displaystyle\int_0^{y_t} g(\nu, h_0, \zeta_0, y)\, \mathrm{d}y\right] & \text{if } y_0 \leqslant y_t \\ \text{else} \\ \Upsilon(\nu - \zeta_0) \exp\left[-L_c \displaystyle\int_0^{y_t} g(\nu, h_0, \zeta_0, y)\, \mathrm{d}y\right] \\ \quad \times \left[\dfrac{1 - \operatorname{erfc}(h_0 + y_t \nu\eta)/2}{1 - \operatorname{erfc}(h_0 + y_0 \nu\eta)/2}\right]^{\Lambda(\nu)} \end{cases} \tag{10}$$

where

$$h_0 = \xi_0/(\omega\sqrt{2}) \qquad \zeta_0 = \gamma_0/(\sigma\sqrt{2}) \qquad y_0 = L_0/L_c, \tag{10a}$$

with $\nu = \cot\theta/(\sigma\sqrt{2})$ and $\eta = \sigma L_c/\omega$, where ω is the surface height standard deviation and L_c the surface correlation length. y_t represents the lower limit of the observation length where the correlation between the surface heights and slopes can be omitted. This means, for the range $y \in [y_t; y_0]$, the correlation can be omitted, meaning that the function $L_c g$ can be analytically integrated over y and gives the second term on the right-hand-side of (10). For $y_0 \leqslant y_t$ the integration of the g function given in table 1 of [26] is computed numerically. It depends on the normalized functions $\{f_{ij}(y)\}$ given by (28a) of [26]

$$\begin{array}{lll} f_{11} = 1 - f_2^2 - f_1^2 & f_{33} = 1 - f_0^2 - f_1^2 & f_{13} = f_1(f_0 - f_2) \\ f_{12} = f_0 f_2^2 + f_1^2 f_2 - f_0 & f_{34} = f_0^2 f_2 + f_1^2 f_0 - f_2 & f_{14} = f_1(1 - f_1^2 - f_0 f_2) \\ f_M = (f_{33}^2 - f_{34}^2)/(1 - f_0^2). & & \end{array} \tag{11}$$

In fact $\{f_{ij}(y)\}$ are equal to $\{C_{iij}\}$ by replacing in (8a) $\{R_0, R_1, R_2, \omega, \sigma\} \rightarrow \{f_0, -f_1, -f_2, 1, 1\}$, where $f_0 = R_0/\omega^2$, $f_1 = -R_1/(\omega\sigma)$ and $f_2 = -R_2/\sigma^2$. For Gaussian and Lorentzian normalized surface height autocorrelation functions, $\{f_0(y)\} = \{\exp(-y^2), 1/(1 + y^2)\}$, $\{f_{1,2}(y)\}$ are given in table 2 of [26], and $\eta = \sigma L_c/\omega = \sqrt{2}$. The $\{f_{ij}(y)\}$ functions are plotted in figure 4 of [26].

When the correlation is neglected we have $f_{ij} = \delta_{ij}$ (Kronecker symbol) with $\delta_{ij} = 1$ if $i = j$ else 0, and $\{y_{tG} = 3, y_{tL} = 4\}$ for Gaussian and Lorentzian correlations. Moreover, the exponential term $\exp[\cdots]$ of (10) is equal to

$$\left[\frac{1 - \operatorname{erfc}(h_0)/2}{1 - \operatorname{erfc}(h_0 + y_0 \nu\eta)/2}\right]^{\Lambda(\nu)}, \tag{11a}$$

and the statistical monostatic shadowing function becomes

$$S(\nu, h_0, \zeta_0, y_0) = \left[\frac{1 - \operatorname{erfc}(h_0)/2}{1 - \operatorname{erfc}(h_0 + y_0 \nu\eta)/2}\right]^{\Lambda(\nu)} \Upsilon(\nu - \zeta_0). \tag{12}$$

The classical function (5) without correlation is then found with $y_0 \nu\eta = \mu L_0/(\sqrt{2}\omega)$ and $h_0 = \xi_0/(\omega\sqrt{2})$. Substituting (10) into (6) with the variable transformations given by (10a) and $p(\xi_0, \gamma_0) = \exp[-\xi_0^2/(2\omega^2) - \gamma_0^2/(2\sigma^2)]/(2\pi\sigma\omega)$, the average shadowing function $S(\nu, y_0)$ can be computed numerically with respect to $\{\nu = \cot\theta/(\sigma\sqrt{2}), y_0 = L_0/L_c\}$.

The comparison in [26] of the uncorrelated and correlated approaches with the numerical exact solution shows that the correlation can be omitted with a good accuracy. The numerical method is obtained from the generation of the surface heights and the use of the algorithm developed by Brokelman and Hagfors [28]. For a finite observation length y_0 [27], the conclusion is similar.

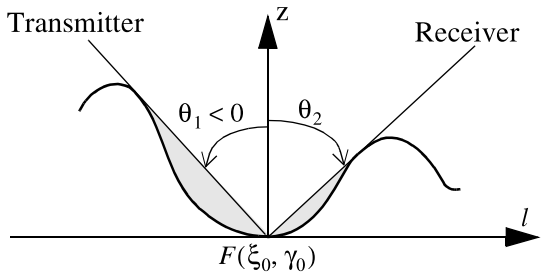

Figure 2. One-dimensional bistatic statistical shadowing function.

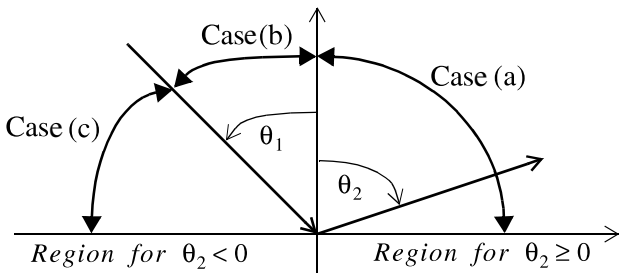

Figure 3. Geometric representation of the three cases for the one-dimensional bistatic configuration.

2.3. Bistatic shadowing function

This section presents the uncorrelated, correlated and numerical statistical bistatic shadowing functions for a one-dimensional rough surface.

From (2.31) of [31], the statistical bistatic shadowing function is given by (figures 2,3)

$$S(\mu_1, \mu_2, F, L_0) = \begin{cases} S(\mu_1, F, L_0)S(\mu_2, F, L_0) & \text{if } \theta_2 \in [0; \pi/2] \quad \text{case(a)} \\ S(\mu_1, F, L_0) & \text{if } \theta_2 \in [\theta_1; 0] \quad \text{case(b)} \\ S(\mu_2, F, L_0) & \text{if } \theta_2 \in [-\pi/2; \theta_1] \quad \text{case(c)}, \end{cases} \tag{13}$$

with $\theta_1 \leqslant 0$. Equation (13) means that the bistatic statistical shadowing function, $S(\mu_1, \mu_2, F, L_0)$, is obtained from two independent monostatic statistical shadowing functions, defined with respect to the locations of the transmitter $S(\mu_1, F, L_0)$ and receiver $S(\mu_2, F, L_0)$.

For any uncorrelated process, Bourlier *et al* show in [26] that (13) becomes

$$S(\nu_1, \nu_2, h_0, \zeta_0, y_0) = \tag{14}$$

$$\Pi\left[\frac{P(h_0) - P(-\infty)}{P(h_0 + \nu_1\eta y_0) - P(-\infty)}\right]^{\Lambda(\nu_1)}\left[\frac{P(h_0) - P(-\infty)}{P(h_0 + \nu_2\eta y_0) - P(-\infty)}\right]^{\Lambda(\nu_2)} \quad \text{if } \nu_2 \geqslant 0, \tag{14a}$$

$$\Upsilon(\nu_1 - \zeta_0)\left[\frac{P(h_0) - P(-\infty)}{P(h_0 + \nu_1\eta y_0) - P(-\infty)}\right]^{\Lambda(\nu_1)} \quad \text{if } -\infty \leqslant -\nu_2 < -\nu_1, \tag{14b}$$

$$\Upsilon(\nu_2 - \zeta_0)\left[\frac{P(h_0) - P(-\infty)}{P(h_0 + \nu_2\eta y_0) - P(-\infty)}\right]^{\Lambda(\nu_2)} \quad \text{if } -\nu_1 \leqslant -\nu_2 < 0, \tag{14c}$$

where

$$\nu_i = |\cot\theta_i|/(\sigma\sqrt{2}),$$
$$\Pi = \begin{cases} 1 & \text{if } \zeta_0 \in [-\nu_1;\, \nu_2] \\ 0 & \text{else} \end{cases}, \qquad \text{and} \qquad \eta = \sigma L_c/\omega. \tag{15}$$

Υ is the Heaviside function defined by (1a), $\{\Lambda, P\}$ is obtained from (3a) and $\{h_0, \zeta_0\}$ denote the surface normalized heights and slopes expressed from (10a).

For an uncorrelated Gaussian process, in (14a)–(14c), the terms between brackets are given by that of (12). For an infinite observation length, the average shadowing function defined as (6) is ((62) of [26])

$$S(\nu_1, \nu_2) = \tag{16}$$

$$[\mathrm{erf}(\nu_1) + \mathrm{erf}(\nu_2)]/\{2[1 + \Lambda(\nu_1) + \Lambda_2(\nu_2)]\} \qquad \text{if } \nu_2 \geqslant 0, \tag{16a}$$
$$[1 + \mathrm{erf}(\nu_1)]/\{2[1 + \Lambda(\nu_1)]\} \qquad \text{if } -\infty \leqslant -\nu_2 < -\nu_1, \tag{16b}$$
$$[1 + \mathrm{erf}(\nu_2)]/\{2[1 + \Lambda(\nu_2)]\} \qquad \text{if } -\nu_1 \leqslant -\nu_2 < 0. \tag{16c}$$

We can note for $\theta_2 \geqslant 0$ that the bistatic average shadowing function $S(\nu_1, \nu_2) \neq S(\nu_1)S(\nu_2)$.

For a correlated Gaussian process, the statistical bistatic shadowing function is ((51) of [26])

$$S(\nu_1, \nu_2, h_0, \zeta_0, y_0) = \tag{17}$$

$$\Pi \exp\left[-L_c \int_0^{y_t} g_{12}(\nu_1, \nu_2, h_0, \zeta_0, y)\,\mathrm{d}y\right]\left[\frac{1 - \mathrm{erfc}(h_0 + y_t\nu_1\eta)/2}{1 - \mathrm{erfc}(h_0 + y_0\nu_1\eta)/2}\right]^{\Lambda(\nu_1)}$$
$$\times \left[\frac{1 - \mathrm{erfc}(h_0 + y_t\nu_2\eta)/2}{1 - \mathrm{erfc}(h_0 + y_0\nu_2\eta)/2}\right]^{\Lambda(\nu_2)} \qquad \text{if } \nu_2 \geqslant 0, \tag{17a}$$

$$\Upsilon(\nu_1 - \zeta_0) \exp\left[-L_c \int_0^{y_t} g(\nu_1, h_0, \zeta_0, y)\,\mathrm{d}y\right]\left[\frac{1 - \mathrm{erfc}(h_0 + y_t\nu_1\eta)/2}{1 - \mathrm{erfc}(h_0 + y_0\nu_1\eta)/2}\right]^{\Lambda(\nu_1)}$$
$$\text{if } -\infty \leqslant -\nu_2 < -\nu_1, \tag{17b}$$

$$\Upsilon(\nu_2 - \zeta_0) \exp\left[-L_c \int_0^{y_t} g(\nu_2, h_0, \zeta_0, y)\,\mathrm{d}y\right]\left[\frac{1 - \mathrm{erfc}(h_0 + y_t\nu_2\eta)/2}{1 - \mathrm{erfc}(h_0 + y_0\nu_2\eta)/2}\right]^{\Lambda(\nu_2)}$$
$$\text{if } -\nu_1 \leqslant -\nu_2 < 0 \tag{17c}$$

where

$$g_{12}(\nu_1, \nu_2, h_0, \zeta_0, y) = g(\nu_1, h_0, \zeta_0, y) + g(\nu_2, h_0, \zeta_0, y). \tag{18}$$

The integration of the g function given in table 1 of [26] is computed numerically. In (17a)–(17c), if $y_0 \leqslant y_t$, then the terms between brackets containing the erfc functions are equal to one. Since (17b), (17c) correspond to a monostatic configuration, they are similar to (10) with ν substituted by either ν_1 for the transmitter or ν_2 for the receiver. Equation (17a) is the product of both monostatic cases defined according to $\{\nu_1, \nu_2\}$.

The numerical average bistatic shadowing function can be computed from the algorithm developed for a monostatic configuration. The algorithm is used both for the transmitter and the receiver, with the fact that a point of the surface is illuminated if it is observed both by the transmitter and the receiver. As the monostatic configuration, comparison of the numerical solution with the uncorrelated and correlated models shows that the uncorrelated statistical shadowing function can be used to a good approximation. This allows us to obtain mathematically a simple statistical shadowing function.

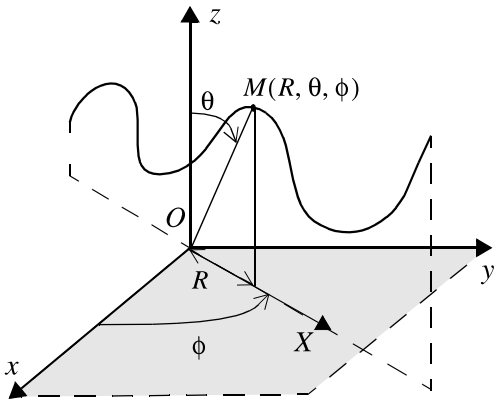

Figure 4. Two-dimensional configuration in polar coordinates.

2.4. Conclusion

In this section, the uncorrelated, correlated and numerical one-dimensional shadowing functions are summarized for monostatic and bistatic configurations with a Gaussian process. Since the Smith formulation is more accurate than Wagner's, only the Smith case is presented in this paper. For an arbitrary uncorrelated process, the statistical shadowing function can be also performed (see (3) and (14)). In general, the correlation can be omitted to a good approximation. In [29], simulation made with a surface slope Laplacian process yields the same conclusion. The purpose of the next section is to extend this approach to an anisotropic two-dimensional surface and quantify the correlation effect on a Gaussian process.

3. Two-dimensional shadowing function

In this section, the two-dimensional shadowing function is investigated for monostatic and bistatic configurations by considering a correlated Gaussian process. To use the results exposed in the second section, the shadowing function is performed in polar coordinates $\{R, \phi\}$ (for a sea surface, ϕ denotes the azimuthal direction according to the wind direction defined along (Ox)). As depicted in figure 4, this approach is similar to making a cross section of the surface along the ϕ direction. As will be shown in this section, since a Gaussian process in Cartesian coordinates remains a Gaussian process in polar coordinates, this rotation allows us to use the set of results presented in the previous section. Mathematically, the covariance matrix defined in Cartesian coordinates has to be calculated in polar coordinates. This method allows us to perform the shadowing effect for a two-dimensional anisotropic surface with an arbitrary uncorrelated process [29].

3.1. Monostatic shadowing function without correlation

The probability density function (pdf) $p(\xi, \gamma)$ of the surface heights ξ and slopes γ defined for a one-dimensional surface becomes, for a two-dimensional surface in the (OX) direction, $p(\xi, \gamma_X)$ where γ_X is the surface slope along the (OX) direction. The covariance matrix $[C_2]$ of $\{\xi, \gamma_X\}$ is defined as

$$[C_2] = \begin{bmatrix} E(\xi^2) & E(\xi\gamma_X) \\ E(\gamma_X\xi) & E(\gamma_X^2) \end{bmatrix}, \tag{19}$$

where $\gamma_X = \gamma_x \cos\phi + \gamma_y \sin\phi$, with $\{\gamma_x, \gamma_y\}$ the surface slopes in the $\{(\mathrm{O}x), (\mathrm{O}y)\}$ directions, and ϕ the azimuthal direction according to $(\mathrm{O}x)$. $E(x)$ denotes the expected value of the random variable x. We can note that $[C_2]$ is a symmetrical matrix, and since the samples $\{\gamma_x, \gamma_y\}$ are Gaussian, γ_X, defined from a sum of $\{\gamma_x, \gamma_y\}$, is also Gaussian. Therefore,

$$E(\xi\gamma_X) = E(\xi[\gamma_x \cos\phi + \gamma_y \sin\phi]) = \cos\phi E(\xi\gamma_x) + \sin\phi E(\xi\gamma_y). \tag{20}$$

Since $\{\xi, \gamma_x, \gamma_y\}$ are assumed to be uncorrelated, we have $E(\xi\gamma_x) = E(\xi\gamma_y) = 0$. Moreover,

$$E(\gamma_X^2) = E([\gamma_x \cos\phi + \gamma_y \sin\phi]^2) = (\sigma_x \cos\phi)^2 + (\sigma_y \sin\phi)^2, \tag{21}$$

where $\{\sigma_x^2, \sigma_y^2\}$ are the slope variances in the $\{(\mathrm{O}x), (\mathrm{O}y)\}$ directions, respectively ($E(\gamma_x\gamma_y) = 0$). With $\omega^2 = E(\xi^2)$ the height variance, the covariance $[C_2]$ can be expressed as

$$[C_2] = \begin{bmatrix} \omega^2 & 0 \\ 0 & \sigma_X^2 \end{bmatrix}, \tag{22}$$

where

$$\sigma_X^2 = (\sigma_x \cos\phi)^2 + (\sigma_y \sin\phi)^2, \tag{22a}$$

which leads to

$$p(\xi, \gamma_X) = \frac{1}{2\pi\omega\sigma_X} \exp\left(-\frac{\gamma_X^2}{2\sigma_X^2} - \frac{\xi^2}{2\omega^2}\right). \tag{23}$$

The pdf $p(\xi, \gamma_X)$ in the ϕ direction is also a Gaussian process with a new slope variance σ_X^2 as a function of ϕ given by (22*a*). We can note, for $\phi = \{0°, 90°\}$, $\sigma_X = \{\sigma_x, \sigma_y\}$. Consequently, for a monostatic configuration with a Gaussian slope pdf, the two-dimensional shadowing effect is obtained from the one-dimensional shadowing effect by replacing in (5*a*) σ by $\sigma_X(\phi)$. We can note in (5) that L_0 becomes the observation length along the ϕ direction.

In figure 5, the two-dimensional average monostatic shadowing function is plotted versus $\{\phi, \theta\}$ for an uncorrelated Gaussian process with $\{\sigma_x = 0.2, \sigma_y = 0.15\}$ (left) and $\{\sigma_x = 0.4, \sigma_y = 0.2\}$ (right). For $\{\sigma_x = 0.2, \sigma_y = 0.15\}$, the shadow increases weakly with ϕ and decreases with θ, because the percentage of the illuminated surface decreases. For $\{\sigma_x = 0.4, \sigma_y = 0.20\}$, the shadow is smaller than the previous case since the slope rms is larger, and the anisotropic effect is more important since the ratio σ_x/σ_y is greater.

3.2. Monostatic shadowing function with correlation

3.2.1. Introduction. For a one-dimensional problem, the surface height $\{\xi, \xi_0\}$ and slope $\{\gamma, \gamma_0\}$ joint conditional pdf $p(\xi, \gamma|\xi_0, \gamma_0; l)$ has to be performed (see (2)). For a two-dimensional problem, in polar coordinates $\{R, \phi\}$, $p(\xi, \gamma|\xi_0, \gamma_0; l)$ becomes $p(\xi, \gamma_X|\xi_0, \gamma_{0X}, ; R, \phi)$. $\{\gamma_{0X}, \gamma_X\}$ are the surface slopes along the $(\mathrm{O}X)$ direction separated by the radial distance R, whereas $\{\xi_0, \xi\}$ are the surface elevations.

The method used in [31] to perform this joint pdf is the following. Firstly, the joint pdf $p(\xi, \gamma_X, \gamma_Y, \xi_0, \gamma_{0X}, \gamma_{0Y}; R, \phi)$ is derived from the knowledge of the joint pdf $p(\xi, \gamma_x, \gamma_y, \xi_0, \gamma_{0x}, \gamma_{0y}; x, y)$ defined in Cartesian coordinates. $\{\gamma_{0x}, \gamma_x\}$ and $\{\gamma_{0y}, \gamma_y\}$ are the surface slopes at the points of coordinates $\{(0, 0), (x, y)\}$, whereas $\{\gamma_{0Y}, \gamma_Y\}$ are the surface slopes in the $(\mathrm{O}X)$ orthogonal direction separated by the radial distance R. Secondly, $p(\xi, \gamma_X, \gamma_Y|\xi_0, \gamma_{0X}, \gamma_{0y}; R, \phi) = p(\xi, \gamma_X, \gamma_Y, \xi_0, \gamma_{0X}, \gamma_{0Y}; R, \phi)/p(\xi_0, \gamma_{0X}, \gamma_{0Y})$ (Bayes theorem) is performed and the joint conditional probability $p(\xi, \gamma_X|\xi_0, \gamma_{0X}; R, \phi)$ is calculated by integrating over γ_Y with $\gamma_{0Y} = \gamma_Y$. With this approach, $p(\xi, \gamma_X|\xi_0, \gamma_{0X}; R, \phi)$

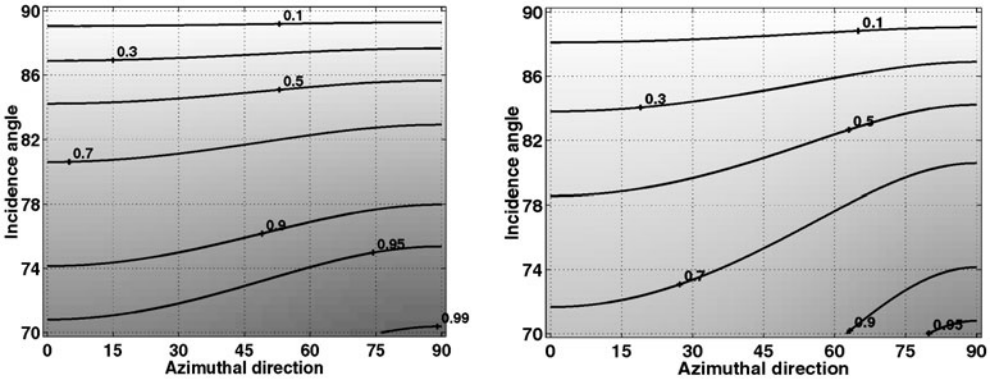

Figure 5. Two-dimensional average monostatic shadowing function versus the azimuthal direction ϕ and the incidence angle θ for an uncorrelated Gaussian process with $\{\sigma_x = 0.2, \sigma_y = 0.15\}$ (left) and $\{\sigma_x = 0.4, \sigma_y = 0.2\}$ (right).

is a complicated function meaning that it does not have the same form as obtained for a one-dimensional surface (see (8)). Therefore, the one-dimensional results cannot be used and the g function has to be re-evaluated. The problem becomes then very complicated. To overcome this problem, another simpler method is required.

To have a similar form as (8), in this paper the joint probability $p(\xi_0, \xi, \gamma_{0X}, \gamma_X; R, \phi)$ is determined by using the same method as the previous section. $p(\xi, \gamma_X|\xi_0, \gamma_{0X}; R, \phi)$ is then equal to $p(\xi_0, \xi, \gamma_{0X}, \gamma_X; R, \phi)/p(\xi_0, \gamma_{0X})$.

3.2.2. Derivation of the covariance matrix. For a six-dimensional Gaussian process, the covariance matrix of $\{\xi_0, \xi, \gamma_{0x}, \gamma_x, \gamma_{0y}, \gamma_y\}$ is

$$[C_6] = \begin{bmatrix} R_0(\mathbf{0}) & R_0 & -R_{1x}(\mathbf{0}) & R_{1x} & -R_{1y}(\mathbf{0}) & R_{1y} \\ R_0 & R_0(\mathbf{0}) & -R_{1x} & -R_{1x}(\mathbf{0}) & -R_{1y} & -R_{1y}(\mathbf{0}) \\ -R_{1x}(\mathbf{0}) & -R_{1x} & -R_{2x}(\mathbf{0}) & -R_{2x} & -R_{2xy}(\mathbf{0}) & -R_{2xy} \\ R_{1x} & -R_{1x}(\mathbf{0}) & -R_{2x} & -R_{2x}(\mathbf{0}) & -R_{2xy} & -R_{2xy}(\mathbf{0}) \\ -R_{1y}(\mathbf{0}) & -R_{1y} & -R_{2xy}(\mathbf{0}) & -R_{2xy} & -R_{2y}(\mathbf{0}) & -R_{2y} \\ R_{1y} & -R_{1y}(\mathbf{0}) & -R_{2xy} & -R_{2xy}(\mathbf{0}) & -R_{2y} & -R_{2y}(\mathbf{0}) \end{bmatrix} \tag{24}$$

with

$$\begin{aligned} R_{1x} &= \frac{\partial R_0}{\partial x} \qquad R_{1y} = \frac{\partial R_0}{\partial y} \\ R_{2x} &= \frac{\partial^2 R_0}{\partial x^2} \qquad R_{2y} = \frac{\partial^2 R_0}{\partial y^2} \qquad R_{2xy} = \frac{\partial^2 R_0}{\partial x\, \partial y}, \end{aligned} \tag{24a}$$

where $R_0(x, y)$ is the surface height autocorrelation function in Cartesian coordinates. To have a real surface without an imaginary part, its spectrum has to be Hermitian, which means that the autocorrelation function $R_0(x, y)$ obtained from the inverse Fourier transform of the spectrum is even according to both $\{(Ox), (Oy)\}$ directions. This means that $R_0(x, y)$ depends on $\{X = x^2, Y = y^2\}$. The even of $R_0(x, y)$ may be obtained with $\{X = |x|, Y = |y|\}$, but $R_0(x, y)$ is not derivable at zero. This implies that $R_{1x}(\mathbf{0}) = 0$, $R_{1y}(\mathbf{0}) = 0$ and $R_{2xy}(\mathbf{0}) = 0$.

Equation (24) becomes then

$$[C_6] = \begin{bmatrix} \omega^2 & R_0 & 0 & R_{1x} & 0 & R_{1y} \\ R_0 & \omega^2 & -R_{1x} & 0 & -R_{1y} & 0 \\ 0 & -R_{1x} & \sigma_x^2 & -R_{2x} & 0 & -R_{2xy} \\ R_{1x} & 0 & -R_{2x} & \sigma_x^2 & -R_{2xy} & 0 \\ 0 & -R_{1y} & 0 & -R_{2xy} & \sigma_y^2 & -R_{2y} \\ R_{1y} & 0 & -R_{2xy} & 0 & -R_{2y} & \sigma_y^2 \end{bmatrix} \tag{25}$$

where $R_0(\mathbf{0}) = \omega^2$ is the height variance, and $\{-R_{2x}(\mathbf{0}) = \sigma_x^2, -R_{2y}(\mathbf{0}) = \sigma_y^2\}$ the slope variances in the up- and cross-directions.

The joint pdf $p(\xi_0, \xi, \gamma_{0X}, \gamma_X; R, \phi)$ is defined by the covariance matrix

$$[C_4] = \begin{bmatrix} E(\xi_0^2) & E(\xi_0\xi) & E(\xi_0\gamma_{0X}) & E(\xi_0\gamma_X) \\ E(\xi_0\xi) & E(\xi^2) & E(\xi\gamma_{0X}) & E(\xi\gamma_X) \\ E(\xi_0\gamma_{0X}) & E(\xi\gamma_{0X}) & E(\gamma_{0X}^2) & E(\gamma_{0X}\gamma_X) \\ E(\xi_0\gamma_X) & E(\xi\gamma_X) & E(\gamma_{0X}\gamma_X) & E(\gamma_X^2) \end{bmatrix}, \tag{26}$$

where $\gamma_{0X,X} = \gamma_{0x,x}\cos\phi + \gamma_{0y,y}\sin\phi$. Since $\{\gamma_{0X,X}\}$ is expressed as the sum of Gaussian slopes $\{\gamma_{0x,x}, \gamma_{0y,y}\}$, the joint pdf $p(\xi_0, \xi, \gamma_{0X}, \gamma_X; R, \phi)$ is also Gaussian. We have

$$E(\xi_0^2) = \omega^2, \tag{26a}$$
$$E(\xi_0\xi) = R_0, \tag{26b}$$
$$E(\xi_0\gamma_{0X}) = \cos\phi E(\xi_0\gamma_{0x}) + \sin\phi E(\xi_0\gamma_{0y}), \tag{26c}$$
$$E(\xi_0\gamma_X) = \cos\phi E(\xi_0\gamma_x) + \sin\phi E(\xi_0\gamma_y), \tag{26d}$$
$$E(\xi^2) = \omega^2, \tag{26e}$$
$$E(\xi\gamma_{0X}) = \cos\phi E(\xi\gamma_{0x}) + \sin\phi E(\xi\gamma_{0y}), \tag{26f}$$
$$E(\xi\gamma_X) = \cos\phi E(\xi\gamma_x) + \sin\phi E(\xi\gamma_y), \tag{26g}$$
$$E(\gamma_{0X}^2) = (\cos\phi)^2 E(\gamma_{0x}^2) + (\sin\phi)^2 E(\gamma_{0y}^2) + \sin(2\phi)E(\gamma_{0x}\gamma_{0y}), \tag{26h}$$
$$E(\gamma_{0X}\gamma_X) = (\cos\phi)^2 E(\gamma_{0x}\gamma_x) + (\sin\phi)^2 E(\gamma_{0y}\gamma_y) + \sin(2\phi)[E(\gamma_{0x}\gamma_y) + E(\gamma_{0y}\gamma_x)]/2, \tag{26i}$$
$$E(\gamma_X^2) = (\cos\phi)^2 E(\gamma_x^2) + (\sin\phi)^2 E(\gamma_y^2) + \sin(2\phi)E(\gamma_x\gamma_y). \tag{26j}$$

The use of (25) yields

$$[C_4] = \begin{bmatrix} \omega^2 & R_0 & 0 & R_1 \\ R_0 & \omega^2 & -R_1 & 0 \\ 0 & -R_1 & \sigma_X^2 & -R_2 \\ R_1 & 0 & -R_2 & \sigma_X^2 \end{bmatrix}, \tag{27}$$

where

$$R_1 = R_{1x}\cos\phi + R_{1y}\sin\phi, \tag{27a}$$
$$R_2 = R_{2x}\sin(\phi)^2 + R_{2y}\cos(\phi)^2 + R_{2xy}\sin(2\phi). \tag{27b}$$

σ_X^2 is given by (22*a*). $R_{0,1,2}$ has to expressed in polar coordinates $\{R, \phi\}$ which means that $\{R_{1x}, R_{1y}, R_{2x}, R_{2y}, R_{2xy}\}$ given by (24*a*) has to depend on $\{R, \phi\}$. The appendix shows that

$$R_1 = \frac{\partial R_0}{\partial R}, \qquad \text{and} \qquad R_2 = \frac{\partial^2 R_0}{\partial R^2}. \tag{28}$$

The conditional joint pdf $p(\xi, \gamma_X|\xi_0, \gamma_{0X}; R, \phi)$ is derived from

$$p(\xi, \gamma_X|\xi_0, \gamma_{0X}; R, \phi) = p(\xi_0, \xi, \gamma_{0X}, \gamma_X; R, \phi)/p(\xi_0, \gamma_{0X}), \tag{29}$$

Table 1. Gaussian and Lorentzian surface height autocorrelation functions for a two-dimensional anisotropic surface. $L_c^2 = [\cos\phi/L_x)^2 + (\sin\phi/L_y)^2]^{-1}$, $L_1^2 = 2L_xL_y/\sin(2\phi)$, $r = R/L_c$ and $l_1 = L_C/L_1$.

	Gaussian case	Lorentzian case
$R_0(x, y)$	$\omega^2 \exp(-x^2/L_x^2 - y^2/L_y^2)$	$\omega^2/(1 + x^2/L_x^2)/(1 + y^2/L_y^2)$
$R_0(R, \phi)$	$\omega^2 \exp(-R^2/L_c^2)$	$\omega^2/(1 + R^2\cos^2\phi/L_x^2)/(1 + R^2\sin^2\phi/L_y^2)$
$R_1(R, \phi) = \dfrac{\partial R_0}{\partial R}$	$-\dfrac{2\omega^2}{L_c^2} R \exp(-R^2/L_c^2)$	$-\dfrac{2\omega^2 R}{L_c^2} \dfrac{(1 + 2R^2L_c^2/L_1^4)}{(1 + R^2/L_c^2 + R^4/L_1^4)^2}$
$R_2(R, \phi) = \dfrac{\partial^2 R_0}{\partial R^2}$	$-\dfrac{2\omega^2}{L_c^2}(1 - 2R^2/L_c^2)\exp(-R^2/L_c^2)$	$\omega^2\left[\dfrac{(2R/L_c^2 + 4R^3/L_1^4)^2}{(1 + R^2/L_c^2 + R^4/L_1^4)^3} - \dfrac{2/L_c^2 + 12R^2/L_1^4}{(1 + R^2/L_c^2 + R^4/L_1^4)^2}\right]$
$\sigma_X, \eta = \sigma_X L_c/\omega$	$2\omega^2/L_c^2, \eta = \sqrt{2}$	$2\omega^2/L_c^2, \eta = \sqrt{2}$
$f_0(r, \phi) = \dfrac{R_0(R, \phi)}{\omega^2}$	$\exp(-r^2)$	$\dfrac{1}{1 + r^2 + (rl_1)^4}$
$f_1(r, \phi) = -\dfrac{R_1(R, \phi)}{\omega\sigma_X}$	$r\sqrt{2}\exp(-r^2)$	$\dfrac{r\sqrt{2}(1 + 2r^2l_1^4)}{[1 + r^2 + (rl_1)^4]^2}$
$f_2(r, \phi) = -\dfrac{R_2(R, \phi)}{\sigma_X^2}$	$(1 - 2r^2)\exp(-r^2)$	$\dfrac{1 + 6r^2l_1^4}{[1 + r^2 + (rl_1)^4]^2} - \dfrac{(2r + 4r^3l_1^4)^2}{[1 + r^2 + (rl_1)^4]^3}$

where the covariance matrix of $p(\xi_0, \gamma_{0X})$ is given by (22). Comparing the covariance matrix (see (9)) performed for a one-dimensional surface with (27), a similar form is found by substituting $\{l, \sigma\} \to \{R, \sigma_X\}$. In (10), the function g for a two-dimensional surface depends now on the ϕ angle within the functions $\{R_{0,1,2}\}$ and $\nu = \cot\theta/(\sigma_X\sqrt{2})$. In addition g depends on $\{f_{ij}\}$ expressed from (11). The last two subsections present them for Gaussian and Lorentzian height correlations and a sea spectrum.

3.2.3. Computation of the $\{f_{ij}\}$ functions for Gaussian and Lorentzian height correlations. Gaussian and Lorentzian height correlations correspond to rough surfaces often used in optics. They are expressed in table 1 with

$$l_1 = L_c/L_1 = \left\{\frac{L_{xy}\sin(2\phi)}{2[(L_{xy}\cos\phi)^2 + (\sin\phi)^2]}\right\}^{1/2}, \qquad \text{where } L_{xy} = L_y/L_x. \tag{30}$$

From table 1, we can see for the two autocorrelation functions that the surface slopes rms σ_X are equal, which means that they have similar uncorrelated shadowing functions since they depend only on the roughness parameter $\nu = \cot\theta/(\sigma_X\sqrt{2})$. On the other hand, for the correlated case, the functions $\{f_{0,1,2}\}$ are different, meaning that $\{f_{ij}\}$ given by (11) and plotted in figure 6 are also different for each autocorrelation function. For the Gaussian autocorrelation function, $\{f_{0,1,2}\}$ are independent of ϕ, but the g function depends on ϕ since ν is as a function of ϕ.

As depicted in figure 6, the functions $\{f_{12}, f_{34}, f_{13}, f_{14}\}(i \neq j)$ become equal to zero when $r \geqslant r_{tG} = 3$ and $r \geqslant r_{tL} = 4$ for Gaussian (chain curve) and Lorentzian (circle and cross curves) cases, respectively, whereas $\{f_{11}, f_{33}\}(i = j)$ become independent of r and tend to unity. In the uncorrelated case represented in the full curve, $\{f_{ij}\}$ is equal to either zero or one. Therefore, in the range $[r_t; \infty[$, the correlation can be neglected, which explains the erfc term of (10), whereas for $[0; r_t]$, $g(\nu, h_0, \zeta_{0X}, r)$ has to be computed numerically from table 1 of [26] with $y = r$ and $\zeta_0 = \zeta_{0X}$.

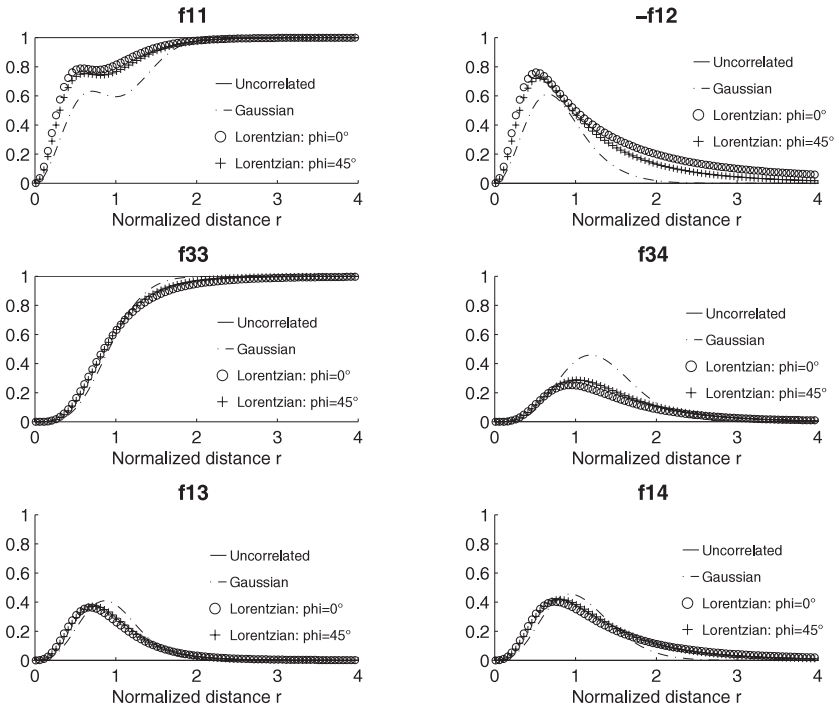

Figure 6. Functions $\{f_{ij}\}$ versus the normalized radial distance r for Gaussian and Lorentzian ($\phi = \{0°, 45°\}$) surface height autocorrelation functions. $L_{xy} = 2$ meaning that $\sigma_x = 2\sigma_y$.

3.2.4. Computation of the $\{f_{ij}\}$ functions for a sea spectrum. This subsection is devoted to correlation functions related to practically important power-type spectra such as sea spectra. The Pierson spectrum [32] is one of the first spectra published in the literature to describe capillary and gravity waves. The gravity region has been modified by adding the JONSWAP behaviour [33] where the fetch effect is provided. Since the capillary region does not fit some physical criteria such as the surface slope variance, its behaviour has been investigated. We can quote the Apel spectrum [34] which is a synthesis of works done in the 1980s and 1990s. Unfortunately, as shown by Elfouhaily *et al* [35], this spectrum does not agree with the slope model proposed by Cox and Munk [36]. This discrepancy is due to an inaccuracy of the capillary waves. The set of these aspects is summarized in [31]. Nevertheless, the Elfouhaily *et al* model was developed without any relation to remote-sensing data. This avoids some deficiencies found in [37].

In fact, all the previous sea roughness spectra have a similar behaviour to describe the gravity waves given by the Pierson–Moskowitz spectrum. In our simulation we use this spectrum defined as

$$S(k, \Theta) = M(k) f(k, \Theta) \tag{31}$$

where

$$M(k) = A \exp(-k_p^2/k^2)/k^3 \qquad k_p = 8.44/u_{19}^2 \qquad A = 4.05 \times 10^{-3}, \tag{31a}$$

$$f(k, \Theta) = [1 + \cos(2\Theta)]/2. \tag{31b}$$

u_{19} denotes the wind speed at an altitude of 19.5 m above the sea. For a sea state equal to

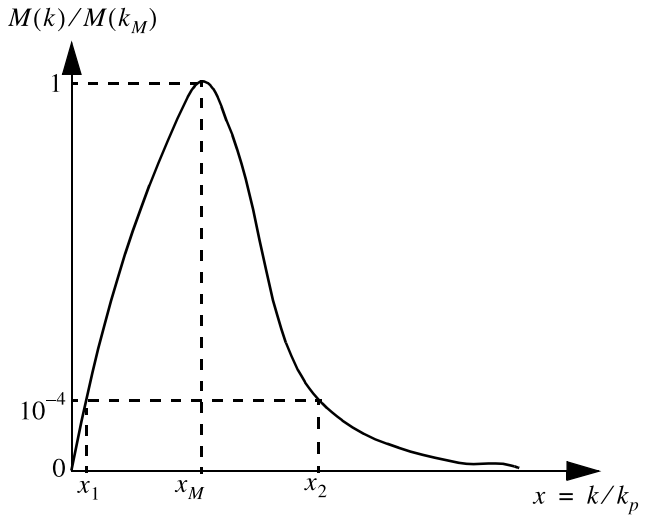

Figure 7. Behaviour of the normalized Pierson–Moskowitz sea spectrum.

six, we get $u_{19} = 11.5$ m s^{-1}. In (31), $M(k)$ denotes the non-directional spectrum (isotropic part) modulated by the $f(k, \Theta)$ spreading function. The general behaviour of the normalized isotropic part $M(k)/M(k_M)$ is depicted in figure 7 versus $x = k/k_p$. $k_M = k_p\sqrt{6}/3 = 0.82k_p$ denotes the wavenumber where the spectrum is a maximum, $k_1 = x_1 k_p = 0.26k_p$ the lower cut-off wavenumber defined as $M(k_1)/M(k_M) = 10^{-4}$ and $k_2 = x_2 k_p = 28.99k_p$ the upper cut-off wavenumber defined as $M(k_2)/M(k_M) = 10^{-4}$.

In Cartesian coordinates, the surface height autocorrelation function $R_0(x, y)$ is equal to the Fourier transform of the spectrum $\Psi(k_x, k_y)$. From (31) and (31*b*), in polar coordinates, the sea autocorrelation function $R_0(R, \phi)$ is expressed from the sea spectrum $S(k, \Theta) = M(k)[1 + \cos(2\Theta)]/2$ as [31]

$$R_0(R, \phi) = R_{00}(R) - \cos(2\phi) R_{02}(R), \tag{32}$$

where

$$R_{00}(R) = \int_{k_1}^{k_2} M(k) J_0(Rk)\,\mathrm{d}k \qquad R_{02}(R) = \int_{k_1}^{k_2} M(k) J_2(Rk)\,\mathrm{d}k. \tag{33}$$

$R_{00}(R)$ is the isotropic part, whereas $R_{02}(R)$ denotes the anisotropic part. J_n is the nth order Bessel function of the first kind. The surface height variance $\omega^2 = R_0(0, \phi) = R_{00}(0)$. The computation of the $\{f_{ij}\}$ functions requires also the knowledge of $\{R_1 = \partial R_0/\partial R, R_2 = \partial R_1/\partial R\}$ and we show

$$R_1(R, \phi) = R_{10}(R) - \cos(2\phi) R_{12}(R), \tag{34}$$

where

$$\begin{aligned} R_{10} &= \frac{\mathrm{d}R_{00}}{\mathrm{d}R} = -\int_{k_1}^{k_2} kM(k) J_1(Rk)\,\mathrm{d}k \\ R_{12} &= \frac{\mathrm{d}R_{02}}{\mathrm{d}R} = \frac{1}{2}\int_{k_1}^{k_2} kM(k)[J_1(Rk) - J_3(Rk)] \end{aligned} \tag{34a}$$

and

$$R_2(R, \phi) = R_{20}(R) - \cos(2\phi) R_{22}(R), \tag{35}$$

Table 2. Calculations of the $\{f_{0,1,2}\}$ functions according to $r = Rk_p$ for a Pierson–Moskowitz roughness spectrum with $M_N(x) = \exp(-1/x^2)/x^3$ and $x = k/k_p$. We can note that $A/(k_p^2\omega^2) = 2/[\exp(-1/x_2^2) - \exp(-1/x_1^2)]$, and $A/(k_p\omega\sigma_X) = (2\sqrt{2})/\{[1 + \cos(2\phi)/2][Ei(1/x_2^2) - Ei(1/x_1^2)][\exp(-1/x_2^2)] - \exp(-1/x_1^2)]\}^{1/2}$ which are independent of $\{A, k_p\}$ like $A/(2\sigma_X^2)$.

$R_{\{0,1,2\}}(R,\phi)$	$R_{0,1,2}(R,\phi) = R_{\{0,1,2\}0}(R) - \cos(2\phi)R_{\{0,1,2\}0}(R)$
$\omega^2 = R_0(0,\phi)$	$A[\exp(-1/x_2^2) - \exp(-1/x_1^2)]/(2k_p^2)$
$\sigma_X^2 = -R_2(0,\phi)$	$A[1 + \cos(2\phi)/2][Ei(1/x_2^2) - Ei(1/x_1^2)]/4$ with $Ei(x) = \int_x^\infty [\exp(-t)/t]\,\mathrm{d}t$
$\eta = \dfrac{\sigma_X L_c}{\omega} = \dfrac{\sigma_X}{k_p\omega}$	$\left\{\dfrac{[1 + \cos(2\phi)/2][Ei(1/x_2^2) - Ei(1/x_1^2)]}{2[\exp(-1/x_2^2) - \exp(-1/x_1^2)]}\right\}^{1/2}$
$f_0(r,\phi) = \dfrac{R_0(R,\phi)}{\omega^2}$	$\dfrac{A}{k_p^2\omega^2}\left[\displaystyle\int_{x_1}^{x_2} M_N(x)J_0(rx)\,\mathrm{d}x - \cos(2\phi)\int_{x_1}^{x_2} M_N(x)J_2(rx)\,\mathrm{d}x\right]$
$f_1(r,\phi) = -\dfrac{R_1(R,\phi)}{\omega\sigma_X}$	$\dfrac{A}{k_p\omega\sigma_X}\left[\displaystyle\int_{x_1}^{x_2} xM_N(x)J_1(rx)\,\mathrm{d}x - \frac{\cos(2\phi)}{2}\int_{x_1}^{x_2} xM_N(x)[J_1(rx) - J_3(rx)]\,\mathrm{d}x\right]$
$f_2(r,\phi) = -\dfrac{R_2(R,\phi)}{\sigma_X^2}$	$\dfrac{A}{2\sigma_X^2}\left[\displaystyle\int_{x_1}^{x_2} x^2M_N(x)[J_0(rx) - J_2(rx)]\,\mathrm{d}x + \frac{\cos(2\phi)}{2}\int_{x_1}^{x_2} x^2M_N(x)[J_0(rx) - 2J_2(rx) + J_4(rx)]\,\mathrm{d}x\right]$

where

$$\begin{aligned} R_{20} &= \frac{\mathrm{d}^2R_{00}}{\mathrm{d}R^2} = -\frac{1}{2}\int_{k_1}^{k_2} k^2M(k)[J_0(Rk) - J_2(Rk)]\,\mathrm{d}k \\ R_{22} &= \frac{\mathrm{d}^2R_{02}}{\mathrm{d}R^2} = \frac{1}{4}\int_{k_1}^{k_2} k^2M(k)[J_0(Rk) - 2J_2(Rk) + J_4(Rk)]\,\mathrm{d}k. \end{aligned} \tag{35a}$$

The surface slope variance $\sigma_X^2(\phi)$ in the ϕ direction is defined as $-R_2(0,\phi) = -[R_{20}(0) - \cos(2\phi)R_{22}(0)]$. Substituting (31*a*) into (33)–(35*a*), the normalized functions $\{f_0, f_1, f_2\}$ are computed numerically versus $\{r = Rk_p, \phi\}$ from integral equations given in table 2. We can observe that $\{f_0, f_1, f_2\}$ are independent of $\{A, k_p\}$ and k_p is similar to the inverse of the surface correlation length L_c.

In figure 8, $\{f_{0,1,2}\}$ are plotted versus the normalized radial distance $r = Rk_p = R/L_c$ for a Pierson–Moskowitz sea spectrum according to $\phi = \{0°, 45°, 90°\}$. Unlike Gaussian and Lorentzian correlations, negative values are observed for f_0 due to the fact that the sea gravity spectrum reaches a maximum located at k_M. This means that the sea spectrum can be expressed as a convolution product of a Dirac distribution centred around k_M by the spectrum centred at zero. The autocorrelation function is then equal to the product of the Fourier transforms of the sea spectrum and the Dirac function, which explains the oscillatory behaviour of f_0. From $\{f_{0,1,2}\}$, $\{f_{ij}\}$ are computed from (11) and $r_t = 12$ since for $r_t \geqslant 12$ we have $\{f_{0,1,2}\} \approx \{0\}$.

3.3. Numerical monostatic shadowing function

To compare the uncorrelated and correlated shadowing functions with an exact solution, the numerical shadowing function has to be computed. For a one-dimensional surface [26] shows that the deviation between the analytical and the numerical solutions is weak, which allows us to conclude that the uncorrelated solution can be used with a good accuracy.

The computation of the numerical shadowing function requires the generation of the surface height samples $z(i)$ computed from $z(i) = b(i)^*w(i)$. b is a Gaussian white noise

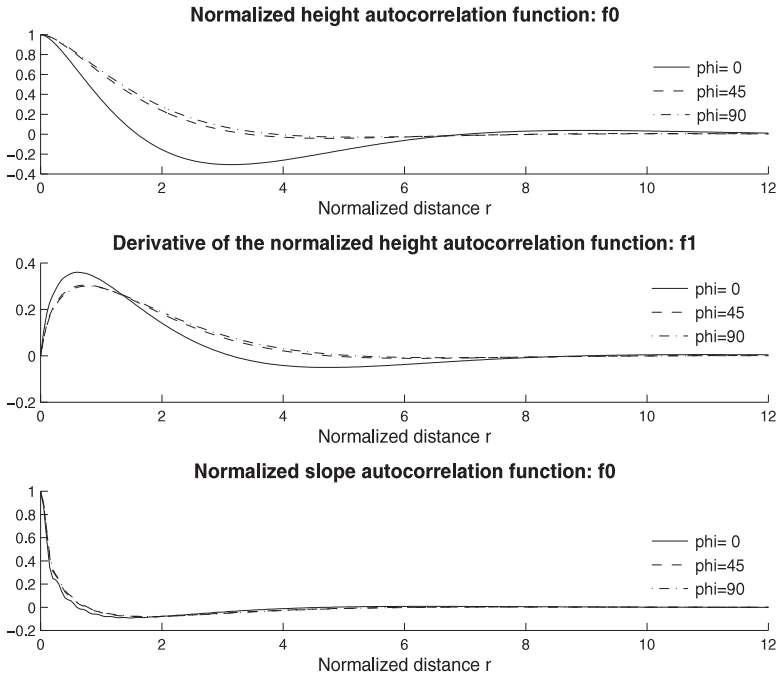

Figure 8. Functions $\{f_{0,1,2}\}$ versus the normalized radial distance $r = Rk_p = R/L_c$ for a Pierson–Moskowitz sea spectrum according to $\phi = \{0°, 45°, 90°\}$.

with zero mean value and unitary variance, the symbol $*$ is the convolution product and w denotes the filter coefficients obtained from the surface height autocorrelation function $R_0(i)$. From [31], $w(i) = \mathrm{FT}^{-1}\{\sqrt{\mathrm{FT}[R_0(i)]}\}$ where FT is the Fourier transform. To have a good representation of the surface statistic such as its autocorrelation function and height distribution, a large number of samples is required such as 100 000. Therefore, for a two-dimensional surface, this method cannot be used since the surface elevation $z(i, j)$ has to be a matrix of dimension $100\,000 \times 100\,000$. Moreover, to compare the analytical solutions with the numerical one, the shadow has to be computed in polar coordinates which require us to interpolate the two-dimensional surface. Another method is therefore used to generate the surface along the azimuthal direction ϕ.

From [30], the surface elevation $\xi(x, y, t)$ can be expressed as a double sum of sinusoidal components from the given energy spectrum $S(k, \Theta)$

$$\xi(x, y, t) = \frac{1}{2\pi} \sum_{i=1}^{N-1} \sum_{j=1}^{M-1} [2S(k_i, \Theta_j)\Delta k \Delta\Theta]^{1/2} \times \cos[k_i(x \cos\Theta_j + y \sin\Theta_j) - \Omega_i t + \Phi_{ij}], \tag{36}$$

with x and y the horizontal directions respectively parallel and normal to the predominant wave direction, t the time, Ω_i the circular frequency, Δk and $\Delta\Theta$ the increments in k and Θ, respectively, and Φ_{ij} a random phase angle uniformly distributed between 0 and 2π. For $t = 0$, in polar coordinates (36) becomes

$$\xi(R, \phi) = \frac{1}{2\pi} \sum_{i=1}^{N-1} \sum_{j=1}^{M-1} [2S(k_i, \Theta_j)\Delta k \Delta\Theta]^{1/2} \cos[k_i R \cos(\Theta_j - \phi) + \Phi_{ij}]. \tag{37}$$

This advantage of this method is to generate the two-dimensional surface in the ϕ direction.

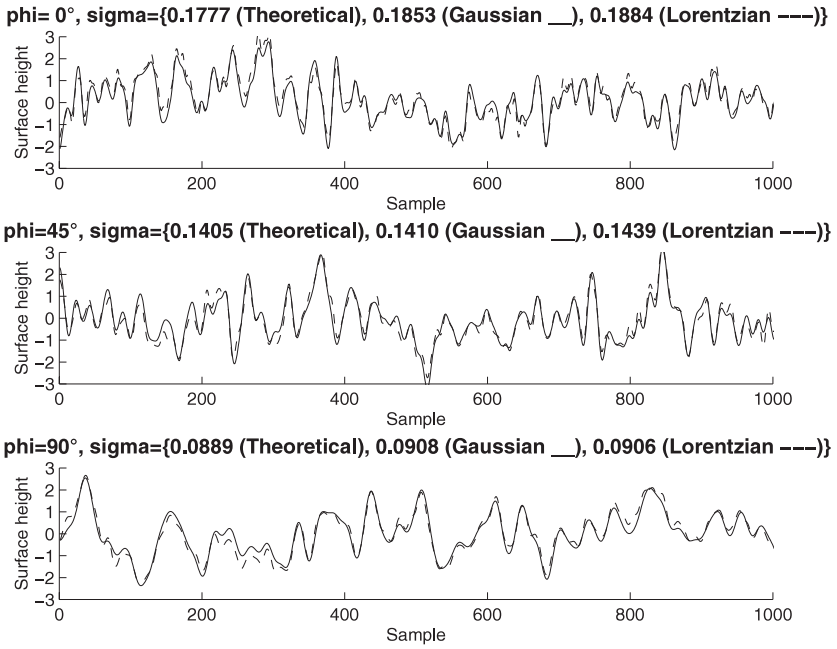

Figure 9. Cross section of the surface heights along the $\phi = \{0°, 45°, 90°\}$ directions, for Gaussian (full curve) and Lorentzian (dashed curve) surface height autocorrelation functions. $\{L_x = 50, L_y = 100\}$, leading to $\sigma_x = 2\sigma_y$. The surface height variance is $\omega = 1$, and the number of the sample is 100 000.

The surface height spectrum defined in Cartesian coordinates $S(k_x, k_y)$ is obtained from the Fourier transform of the surface height autocorrelation function $R_0(x, y)$, yielding

$$S(k_x, k_y) = \int_{-\infty}^{\infty}\int_{-\infty}^{\infty} R_0(x, y)\exp[-\mathrm{j}(k_x x + k_y y)]\,\mathrm{d}x\,\mathrm{d}y. \tag{38}$$

For Gaussian (subscript G) and Lorentzian (subscript L) autocorrelation functions given in table 1, we get

$$\begin{aligned} S_G(k_x, k_y) &= \pi L_x L_y \exp[-(k_x L_x/2)^2 - (k_y L_y/2)^2] \\ S_L(k_x, k_y) &= \pi^2 L_x L_y \exp(-|k_x|L_x - |k_y|L_y). \end{aligned} \tag{39}$$

The spectrum $S(k, \Theta)$ defined in polar coordinates is obtained from the one expressed in Cartesian coordinates by writing $S(k_x, k_y)\,\mathrm{d}k_x\,\mathrm{d}k_y = kS(k, \Theta)\,\mathrm{d}k\,\mathrm{d}\Theta$ with $k_x = k\cos\Theta$ and $k_y = k\sin\Theta$. For a sea surface, the Pierson–Moskowitz spectrum given by (31) is used.

Figure 9 represents the cross section of the surface heights along the $\phi = \{0°, 45°, 90°\}$ directions, for Gaussian and Lorentzian surface height autocorrelation functions. The correlation lengths are $\{L_x = 50, L_y = 100\}$, the surface height variance is $\omega = 1$ and the number of samples is 100 000. In (37), $N = M = 100$. For a given ϕ, we can see that the surfaces are similar.

In figure 10, the surface height and slope normalized histograms of the surfaces (plotted in figure 9) are depicted versus the surface heights and normalized surface slopes, respectively. We can observe that both surface heights and slopes obey a Gaussian process with one height standard deviation and $\sigma_X = \omega\sqrt{2}/L_c$ (see table 1) slope standard deviation for both autocorrelation functions. Comparison of the numerical slope rms with the theoretical one (see figure 9) gives good agreement, with a weak overestimation of the order of 4%.

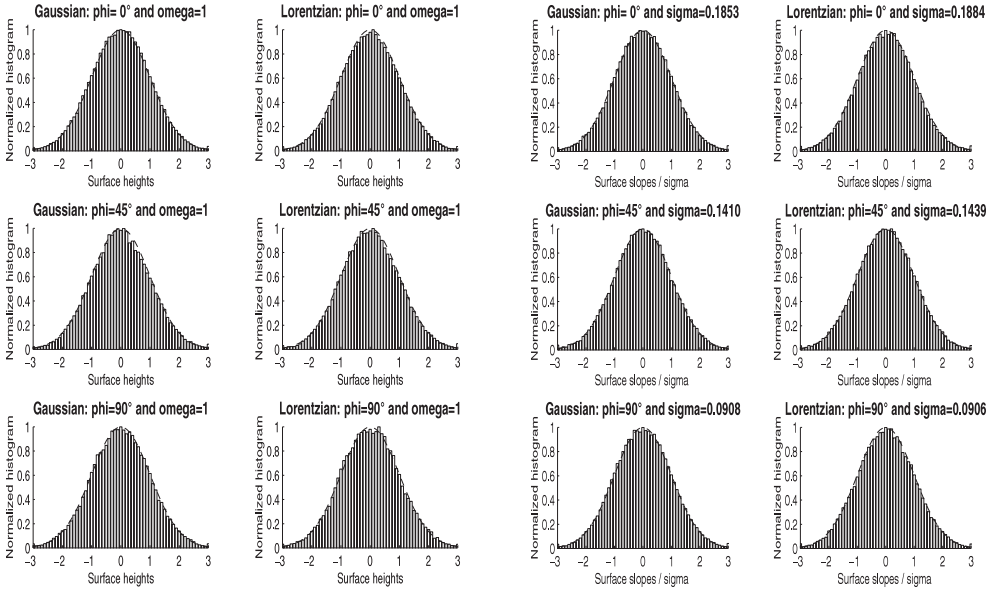

Figure 10. On the left, the normalized histograms of the surface heights plotted in figure 9. On the right, the normalized histograms of the surface slopes obtained from the surface heights plotted in figure 9.

For a Pierson–Moskowitz roughness spectrum, on the left of figure 11, the surface height is plotted with a wind speed $u_{19} = 11.5\ \mathrm{m\,s^{-1}}$. In (37), $\{N = 200, M = 100\}$, and the number of samples is 100 000. In the middle, the normalized histogram of the surface heights. On the right, the normalized histogram of the surface slopes. The wind direction is $\phi = \{0°, 45°, 90°\}$. As previously, a good fit is observed between the numerical and theoretical distributions. For the normalized histograms, the first values of $\{\omega, \sigma_X\}$ are numerical and the second ones are theoretical.

3.4. Comparison of the average monostatic shadowing functions

In this subsection, the uncorrelated, correlated and numerical average shadowing functions are compared for a Gaussian surface and an infinite observation length ($r_0 \to \infty$).

The uncorrelated one $S_{unc}(\nu, \infty)$ is given by (7) with $\nu = \cot\theta/[\sigma_X(\phi)\sqrt{2}]$. The correlated one $S_{cor}(\nu, r_0)$ (r_0 is the normalized observation length according to the surface correlation length L_C), is computed from the substitution of (10) into (6) with the variable transformations given by (10*a*). This leads to

$$S_{cor}(\nu, r_0) = \begin{cases} \displaystyle\int_{-\infty}^{\infty} \exp(-h_0^2) G(\nu, h_0, r_t)\, \mathrm{d}h_0 & \text{if } r_0 \leqslant r_t \\ \displaystyle\int_{-\infty}^{\infty} \exp(-h_0^2) \left[\frac{1 - \mathrm{erfc}(h_0 + r_t \nu\eta)/2}{1 - \mathrm{erfc}(h_0 + r_0 \nu\eta)/2}\right]^{\Lambda(\nu)} G(\nu, h_0, r_t)\, \mathrm{d}h_0 & \text{else} \end{cases} \tag{40}$$

where

$$G(\nu, h_0, r_t) = \int_{-\infty}^{\nu} \exp(-\zeta_{0X}^2) \exp\left[-L_c \int_0^{r_t} g(\nu, h_0, \zeta_{0X}, r)\, \mathrm{d}r\right] \mathrm{d}\zeta_{0X}. \tag{40a}$$

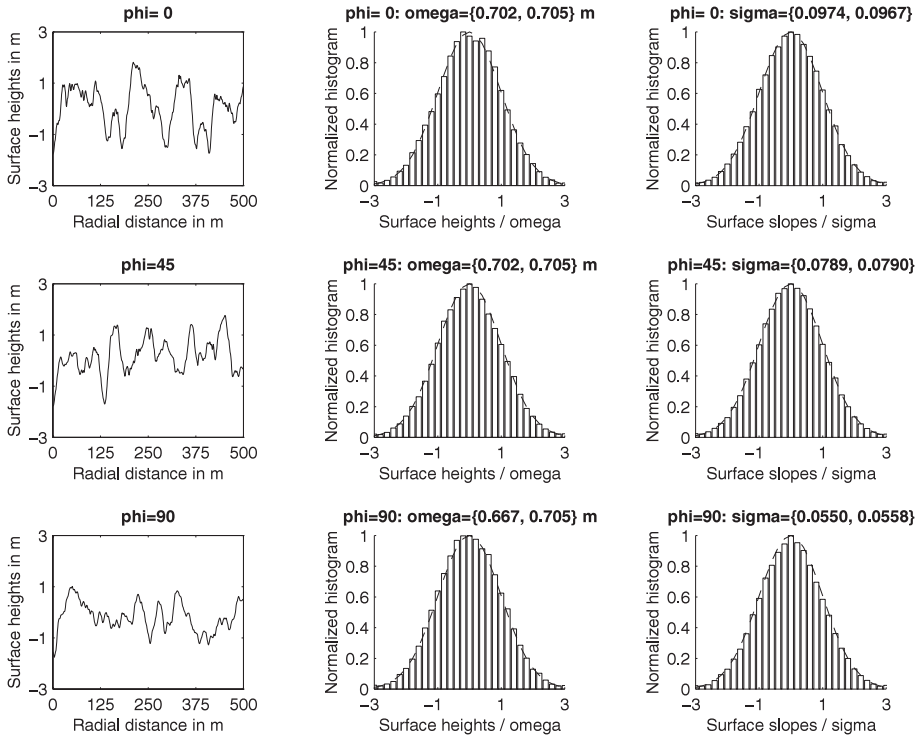

Figure 11. On the left, surface heights for a Pierson–Moskowitz roughness spectrum with a wind speed $u_{19} = 11.5$ m s^{-1}. In the middle, the normalized histogram of the surface heights. On the right, the normalized histogram of the surface slopes. The wind direction is $\phi = \{0°, 45°, 90°\}$.

The function $L_c g$ is expressed in table 1 of [26] and computed numerically. It depends on the normalized functions $\{f_{ij}(y)\}$, given by (11), where $\{f_0, f_1, f_2, \eta\}$ are expressed in table 1 for Gaussian ($r_t = 3$, see figure 6) and Lorentzian ($r_t = 4$, see figure 6) autocorrelation functions, and in table 2 for a Pierson–Moskowitz sea spectrum ($r_t = 12$, see figure 8). The numerical average shadowing function S_{num} is computed from the generation of the surface heights, and with the help of the algorithm developed by Brokelman and Hagfors [28] summarized in figure 5 of [26].

In figures 12 and13, the differences $\{S_{unc} - S_{num}, S_{cor} - S_{num}\}$ between the numerical solution and the uncorrelated (at the top) and correlated (at the bottom) average monostatic shadowing functions are plotted versus the azimuthal direction ϕ and the incidence angle θ. The left-hand side corresponds to the Gaussian correlation case, and the right-hand side to the Lorentzian one. In figure 12 $\{\sigma_x = 0.4, \sigma_y = 0.2\}$, whereas in figure 13 the rms slopes are divided by two $\{\sigma_x = 0.2, \sigma_y = 0.1\}$. Within the values of the extrema {min, max}, we can observe that the differences are small. For the uncorrelated case (at the top), the results are weakly overpredicted ($S_{unc} > S_{num}$), whereas for the correlated ones (at the bottom), they are slightly underestimated ($S_{cor} < S_{num}$). Since for figure 13 the surface slope is divided by two, the difference becomes significant for incidence angles greater than the one observed in figure 12, where the shadowing effect is more important.

In figure 14, the numerical, correlated and uncorrelated monostatic shadowing functions are represented versus the incidence angle for a Pierson–Moskowitz sea spectrum with a wind speed $u_{19} = 11.5$ m s^{-1}. At the top, $\phi = 0$. In the middle, $\phi = 45°$. At the bottom $\phi = 90°$.

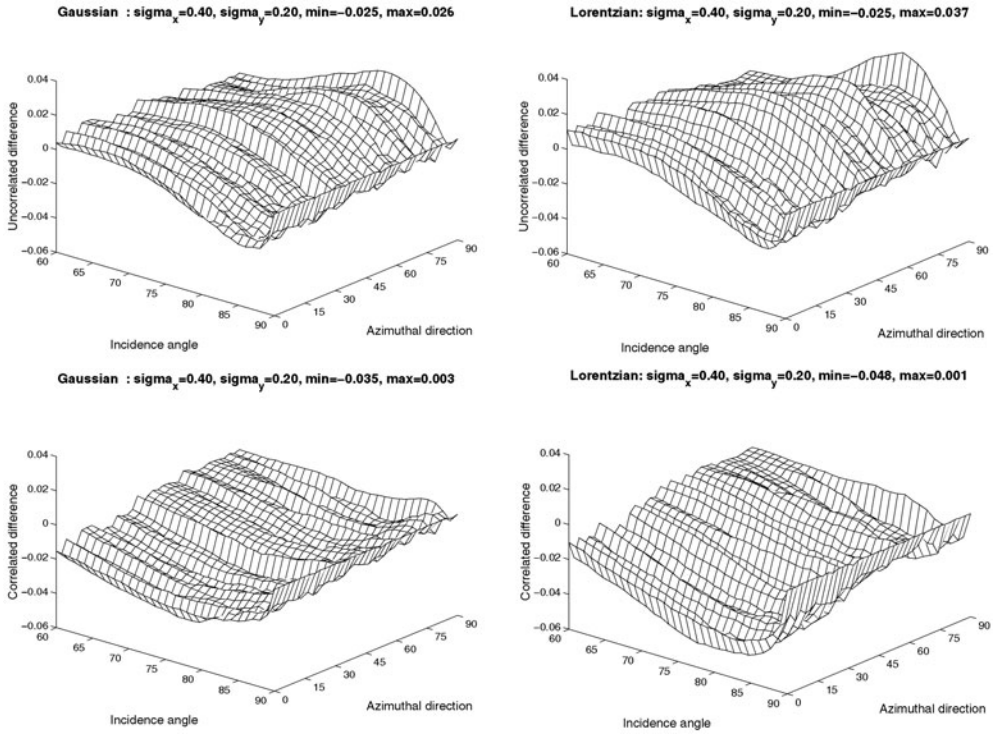

Figure 12. Differences $\{S_{unc} - S_{num}, S_{cor} - S_{num}\}$ between the numerical solution and the uncorrelated (at the top) and correlated (at the bottom) average monostatic shadowing functions for Gaussian (on the left) and Lorentzian (on the right) autocorrelation functions, with $\{\sigma_x = 0.4, \sigma_y = 0.2\}$.

As previously, we can note that the correlated results are slightly smaller than the numerical ones and the uncorrelated model is close to the numerical solution.

3.5. Average bistatic shadowing function

As shown in figure 15, for a bistatic configuration the transmitter and the receiver are located by the knowledge of the azimuthal directions $\{\phi_1, \phi_2\}$ along the (Ox) direction and the incidence angles $\{\theta_1, \theta_2\}$.

3.5.1. Receiver and transmitter located in the same plane. When the transmitter and receiver are in the same plane, we have $\phi_2 = \phi_1$ and the surface slopes viewed by the transmitter and receiver are equal. Since, for a two-dimensional Gaussian surface, the process remains also Gaussian in polar coordinates, the uncorrelated statistical bistatic shadowing function is similar to the one (see (14)) performed for a one-dimensional Gaussian surface. We can also note in (14) that $\nu_i = |\cot\theta_i|/[\sigma_X(\phi_i)\sqrt{2}]$, and the normalized surface length y_0 becomes $\{r_{01}, r_{02}\}$ according to the transmitter and the receiver, respectively. From (22a), we have $\sigma_X^2(-\phi_i) = \sigma_X^2(\phi_i)$, which explains that $\phi_2 \in [0; \pi/2]$. This means that the (Ox) direction is a symmetric axis.

In figure 16, for infinite normalized observation lengths, $\{r_{01}, r_{02}\} \to \infty$, the uncorrelated average bistatic shadowing function $S_{unc}(\nu_1, \nu_2)$ given by (16) is plotted versus

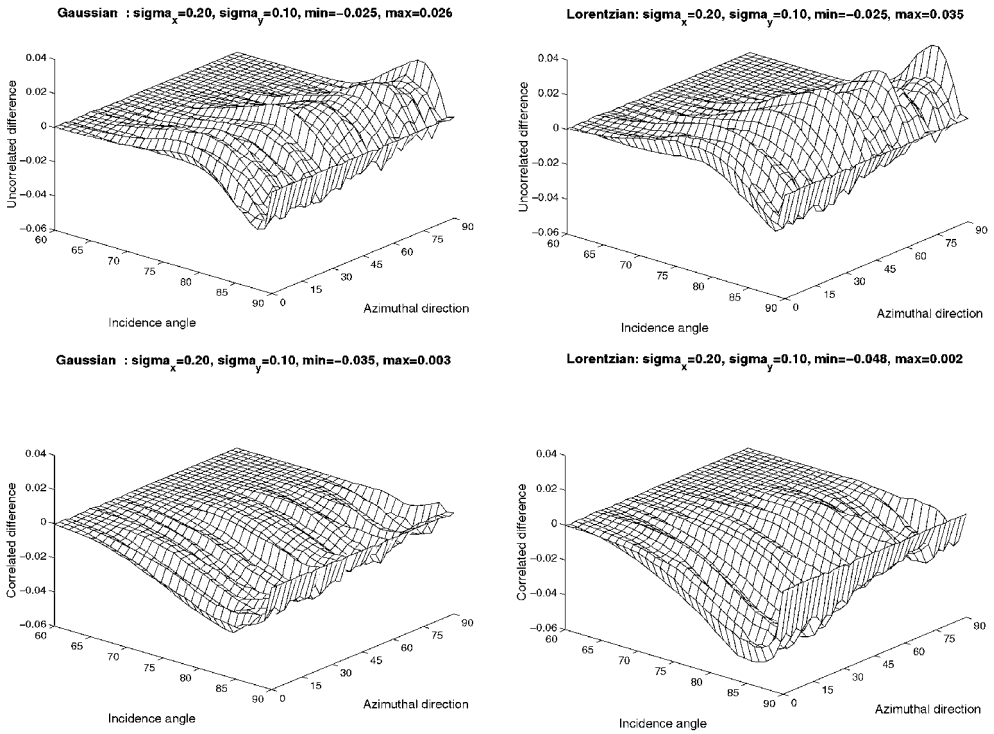

Figure 13. The same variation as in figure 12 with $\{\sigma_x = 0.2, \sigma_y = 0.1\}$.

the azimuthal direction ϕ_2 and the incidence angle θ_2, with $\{\sigma_x = 0.4, \sigma_y = 0.2\}$ and $\theta_1 = \{-70, -75, -80, -85\}$. We can see that the shadow equal to the percentage of the illuminated surface increases with ϕ_2 because the surface is less rough ($\sigma_X(\phi_i)$ decreases) and decreases with $|\theta_2|$ and $|\theta_1|$.

In the correlated case, the statistical bistatic shadowing function is given by (17). For $\theta_2 < 0$ ((17*b*) and (17*c*)), the configuration is monostatic, simulated previously. Therefore, only the case $\theta_2 \geqslant 0$ is studied. The substitution of (17*a*) into (6) with the variable transformations given by (10*a*) yields for infinite observation lengths

$$S_{cor}(\nu_1, \nu_2) = \int_{-\infty}^{\infty} \exp(-h_0^2) G_{12}(\nu_1, \nu_2, h_0, r_t) \{[1 - \operatorname{erfc}(h_0 + r_t \nu_1 \eta)]/2\}^{\Lambda(\nu_1)} \times \{[1 - \operatorname{erfc}(h_0 + r_t \nu_2 \eta)]/2\}^{\Lambda(\nu_2)} \, \mathrm{d}h_0, \tag{41}$$

where

$$G_{12}(\nu_1, \nu_2, h_0, r_t) = \int_{-\nu_1}^{\nu_2} \exp(-\zeta_{0X}^2) \exp\left[-L_c \int_0^{r_t} g_{12}(\nu_1, \nu_2, h_0, \zeta_{0X}, r) \, \mathrm{d}r\right] \mathrm{d}\zeta_{0X}, \tag{41a}$$

and g_{12} is expressed from (18). The numerical bistatic shadowing function is computed from [26].

In figures 17 and18, the differences $\{S_{unc} - S_{num}, S_{cor} - S_{num}\}$ between the numerical solution represented in figure 19 and the uncorrelated and correlated average bistatic shadowing functions are plotted versus the azimuthal direction ϕ_2 and the incidence angle $\theta_2 \cdot \{\sigma_x = 0.4, \sigma_y = 0.2\}$, $\theta_1 = \{-55°, -65°, -75°, -85°\}$, and the correlation is Gaussian. As in the monostatic case (figures 12, 13), the correlated results (figure 18) underpredict

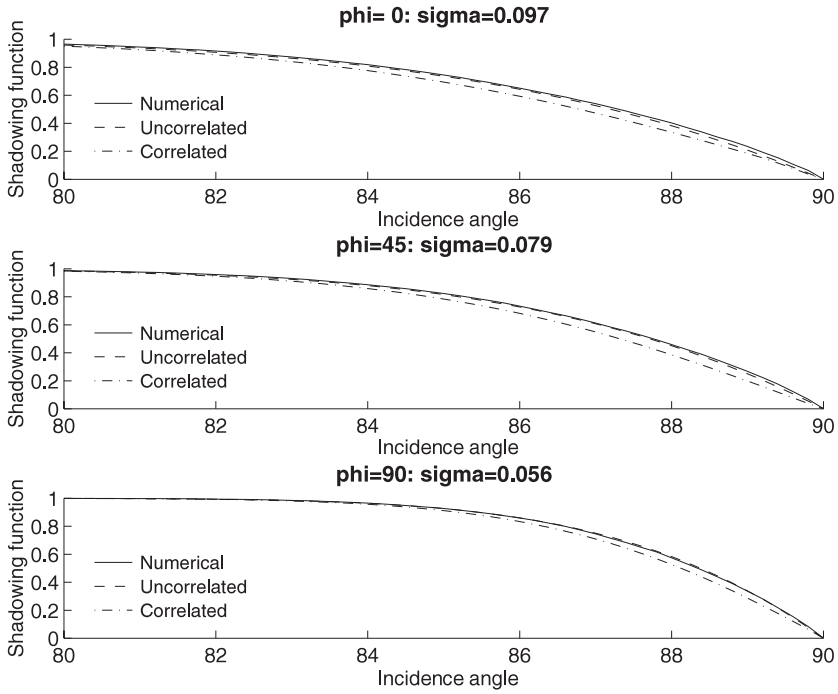

Figure 14. Numerical, correlated and uncorrelated monostatic shadowing functions versus the incidence angle for a Pierson–Moskowitz sea spectrum with a wind speed $u_{19} = 11.5$ m s^{-1}. At the top, $\phi = 0$. In the middle, $\phi = 45°$. At the bottom $\phi = 90°$.

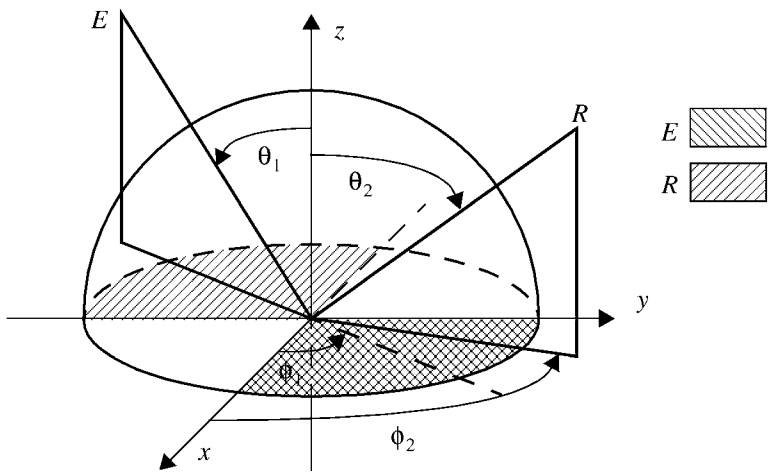

Figure 15. Bistatic shadowing function for a two-dimensional surface. $\phi_1 \in [-\pi/2; 0]$ and $\theta_1 \in [-\pi/2; 0]$. $\phi_2 \in [-\pi/2; \pi/2]$ and $\theta_2 \in [-\pi/2; \pi/2]$. The hatched zones represent the spaces covered by the transmitter and the receiver.

weakly the shadow whereas the uncorrelated solution (figure 17) overestimates them. We can also note that the difference $S_{cor} - S_{num}$ increases with the incidence angle $|\theta_1|$ although the shadowing function is small (see figure 19). Other simulations not presented in this paper lead to the same conclusion.

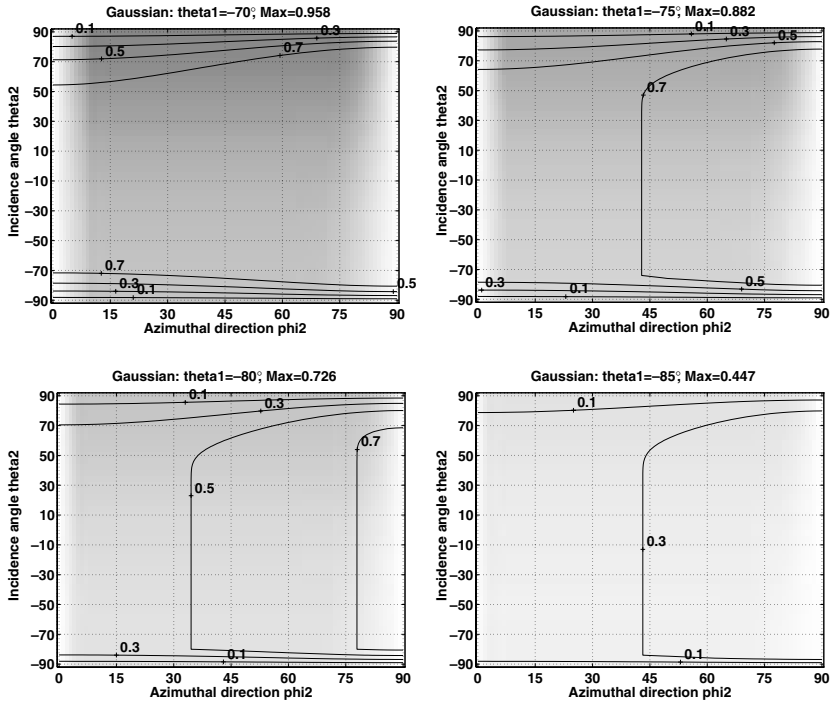

Figure 16. Two-dimensional average bistatic shadowing function versus the azimuthal direction ϕ_2 and the incidence angle θ_2 for an uncorrelated Gaussian process with $\{\sigma_x = 0.4, \sigma_y = 0.2\}$ and $\theta_1 = \{-70, -75, -80, -85\}$. The transmitter and the receiver are assumed to be located in the same plane.

For the computations of the numerical and correlated shadowing functions, only the case of Gaussian autocorrelation is studied, since with a sea spectrum and Lorentzian correlation, we have a similar conclusion for a monostatic configuration.

3.5.2. Transmitter and receiver located in different planes. As shown in figure 20, if the transmitter and receiver are located in different planes, the surface slopes $\{\gamma_{0X_1}, \gamma_{0X_2}\}$ viewed by the transmitter and the receiver are then not equal, meaning that the statistical bistatic shadowing function $S(\{\theta_i, \phi_i, \xi_0, \gamma_{0X_i}, L_{0i}\})(i = \{1, 2\})$ is

$$S(\{\theta_i, \phi_i, \xi_0, \gamma_{0X_i}, L_{0i}\}) = \prod_{i=1}^{i=2} S(\theta_i, \phi_i, \xi_0, \gamma_{0X_i}, L_{0i}), \tag{42}$$

where $\{S(\theta_i, \phi_i, \xi_0, \gamma_{0X_i}, L_{0i})\}$ denote the statistical monostatic shadowing functions defined according to the transmitter (subscript 1) and the receiver (subscript 2). $\{L_{0i}\}$ are the observation lengths along the (OX_i) directions and ξ_0 the surface elevations.

The average bistatic shadowing function $S(\{\theta_i, \phi_i, L_{0i}\})$ integrated over $\{\xi_0, \gamma_{0X_1}, \gamma_{0X_2}\}$ is then

$$S(\{\theta_i, \phi_i, L_{0i}\}) = \int_{-\infty}^{\infty}\int_{-\infty}^{\infty}\int_{-\infty}^{\infty} p(\xi_0, \gamma_{0X_1}, \gamma_{0X_2}) S(\{\theta_i, \phi_i, \xi_0, \gamma_{0X_i}, L_{0i}\})\, \mathrm{d}\xi_0\, \mathrm{d}\gamma_{0X_1}\, \mathrm{d}\gamma_{0X_2}. \tag{43}$$

When the transmitter and the receiver are in the same plane, we have $\gamma_{0X_1} = \gamma_{0X_2} = \gamma_{0X}$. Therefore, the bistatic statistical shadowing function is only integrated over $\{\xi_0, \gamma_{0X}\}$.

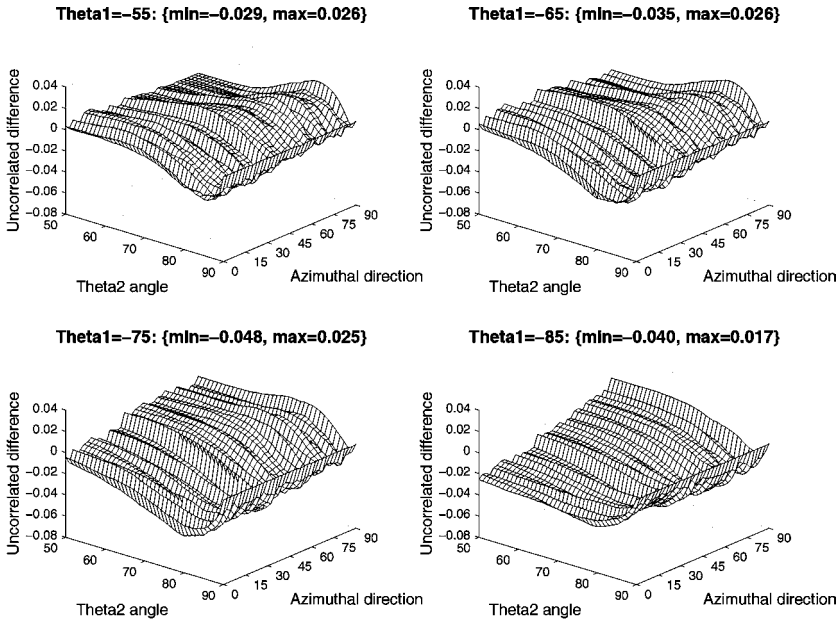

Figure 17. Differences $S_{unc} - S_{num}$ between the numerical solution (plotted in figure 19) and the uncorrelated average bistatic shadowing function for the Gaussian autocorrelation function, with $\{\sigma_x = 0.4, \sigma_y = 0.2\}$ and $\theta_1 = \{-55°, -65°, -75°, -85°\}$. The transmitter and the receiver are located in the same plane.

The covariance matrix $[C_3]$ of samples $\{\xi_0, \gamma_{0x}, \gamma_{0y}\}$ corresponds to the partitioned matrix $[C_6]$ (lines and columns 1, 3 and 5) of (25)

$$[C_3] = \begin{bmatrix} \omega^2 & 0 & 0 \\ 0 & \sigma_x^2 & 0 \\ 0 & 0 & \sigma_y^2 \end{bmatrix}. \tag{44}$$

Using the same method as section 3.2.2, the covariance matrix $[R_3]$ of samples $\{\xi_0, \gamma_{0X_1}, \gamma_{0X_2}\}$ is then

$$[R_3] = \begin{bmatrix} \omega^2 & 0 & 0 \\ 0 & \sigma_{X_1}^2 & \rho\sigma_{X_1}\sigma_{X_2} \\ 0 & \rho\sigma_{X_1}\sigma_{X_2} & \sigma_{X_2}^2 \end{bmatrix}, \tag{45}$$

where

$$\sigma_{X_i}^2 = E(\gamma_{0X_i}^2) = \sigma_X^2(\phi_i), \tag{45a}$$

$$\rho = \frac{E(\gamma_{0X_1}\gamma_{0X_2})}{[E(\gamma_{0X_1}^2)E(\gamma_{0X_2}^2)]^{1/2}} = \frac{\sigma_x^2 \cos\phi_1 \cos\phi_2 + \sigma_y^2 \sin\phi_1 \sin\phi_2}{\sigma_{X_1}\sigma_{X_2}}. \tag{45b}$$

Since $E(\xi_0\gamma_{0x}) = E(\xi_0\gamma_{0y}) = 0$, we get $E(\xi_0\gamma_{0X_1}) = E(\xi_0\gamma_{0X_2}) = 0$. Thus, for a Gaussian process, we obtain

$$p(\xi_0, \gamma_{0X_1}, \gamma_{0X_2}) = \frac{\exp[-\frac{\xi_0^2}{2\omega^2} - \frac{1}{2(1-\rho^2)\sigma_{X_1}^2\sigma_{X_2}^2}(\gamma_{0X_1}^2\sigma_{X_2}^2 + \gamma_{0X_2}^2\sigma_{X1}^2 - 2\rho\gamma_{0X_1}\gamma_{0X_2}\sigma_{X_1}\sigma_{X_2})]}{(2\pi)^{3/2}\omega\sigma_{X_1}\sigma_{X_2}(1-\rho^2)^{1/2}}. \tag{46}$$

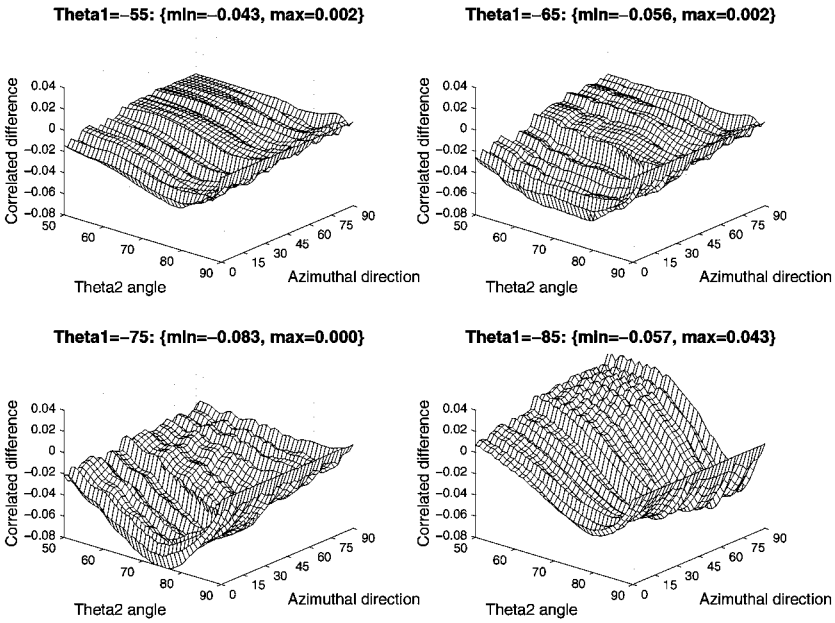

Figure 18. Differences $S_{cor} - S_{num}$ between the numerical solution (plotted in figure 19) and the correlated average bistatic shadowing function for the Gaussian autocorrelation function, with $\{\sigma_x = 0.4, \sigma_y = 0.2\}$ and $\theta_1 = \{-55°, -65°, -75°, -85°\}$. The transmitter and the receiver are located in the same plane.

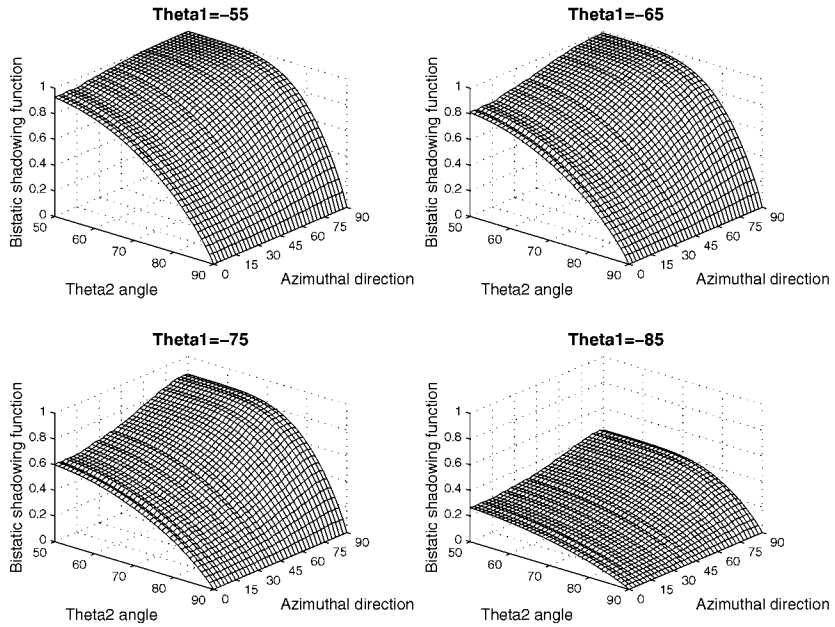

Figure 19. Numerical bistatic shadowing function for the Gaussian autocorrelation function, with $\{\sigma_x = 0.4, \sigma_y = 0.2\}$ and $\theta_1 = \{-55°, -65°, -75°, -85°\}$. The transmitter and the receiver are located in the same plane.

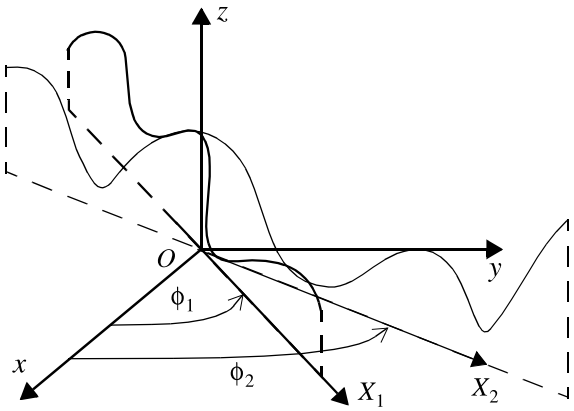

Figure 20. Case where the transmitter and the receiver are not located in the same plane.

For an uncorrelated Gaussian process, the statistical monostatic shadowing function $S(\theta_i, \phi_i, \xi_0, \gamma_{0X_i}, L_{0i})$ is given from (5) swapping $\{\mu, L_0, \nu, \gamma_0\}$ for $\{\mu_i = \cot|\theta_i|, L_{0i}, \nu_i = \mu_i/[\sigma_X(\phi_i)\sqrt{2}], \gamma_{0X_i}\}$, respectively. For an infinite observation length, S becomes

$$S(\theta_i, \phi_i, \xi_0, \gamma_{0X_i}) = \Upsilon(\mu_i - \gamma_{0X_i})\{1 - \operatorname{erfc}[\xi_0/(\sqrt{2}\omega)]/2\}^{\Lambda(\nu_i)}. \tag{47}$$

Substituting (47) and (46) into (43) and integrating over ξ_0, we have for infinite observation lengths $\{L_{0i} \to \infty\}$

$$S(\{\theta_i, \phi_i\}) = \frac{\int_{-\infty}^{\mu_1} \mathrm{d}\gamma_{0X_1} \int_{-\infty}^{\mu_2} \exp[-\frac{\gamma_{0X_1}^2\sigma_{X_2}^2 + \gamma_{0X_2}^2\sigma_{X1}^2 - 2\rho\gamma_{0X_1}\gamma_{0X_2}\sigma_{X_1}\sigma_{X_2}}{2(1-\rho^2)\sigma_{X_1}^2\sigma_{X_2}^2}]\,\mathrm{d}\gamma_{0X_2}}{2\pi\sigma_{X_1}\sigma_{X_2}(1-\rho^2)^{1/2}[1 + \Lambda(\nu_1) + \Lambda(\nu_2)]}. \tag{48}$$

The variable transformations $\gamma_{0X_2} = x_2\sigma_{X_2}[2(1-\rho^2)]^{1/2}$, $\gamma_{0X_1} = x_1\sigma_{X_1}\sqrt{2}$, and the integration over x_2 lead to

$$S(\{\theta_i, \phi_i\}) = \frac{\int_{-\infty}^{\nu_1} \exp(-x_1^2)\{1 + \operatorname{erf}[(\nu_2 - \rho x_1)/(1-\rho^2)^{1/2}]\}\,\mathrm{d}x_1}{[1 + \Lambda(\nu_1) + \Lambda(\nu_2)]2\sqrt{\pi}}. \tag{49}$$

The integration over x_1 is computed numerically. If the correlation between $\{\gamma_{0X_1}, \gamma_{0X_2}\}$ is neglected, then $\rho = 0$, and the above equation becomes $[1 + \operatorname{erf}(\nu_1)][1 + \operatorname{erf}(\nu_2)]/\{4[1 + \Lambda(\nu_1) + \Lambda(\nu_2)]\}$. In [29], this assumption is used.

In figure 21, the two-dimensional average bistatic shadowing function $S(\{\theta_i, \phi_i\})$ is plotted versus the azimuthal directions $\{\phi_1, \phi_2\}$ for an uncorrelated Gaussian process with $\{\sigma_x = 0.4, \sigma_y = 0.2\}$, $\theta_2 = \{-85°, -60°, 85°, 60°\}$ and $\theta_1 = -75°$. For $\theta_2 < 0$ (figures (a) and (b)), if $\phi_2 = \phi_1$ then $S(\{\theta_i, \phi_i\})$ is computed from either (16*b*) (case where $|\theta_1| > |\theta_2|$) or (16*c*) (case where $|\theta_1| < |\theta_2|$) which is greater than (49) used for $\phi_2 \neq \phi_1$. For $\theta_2 > 0$ (figures (c) and (d)) with $\phi_2 = \phi_1$, the shadow is given by (16*a*).

For the correlation case with infinite observation lengths, the average bistatic shadowing function is expressed from (41), where G_{12} is given by

$$G_{12}(\nu_1, \nu_2, h_0, r_t) = \int_{-\infty}^{\nu_1} \mathrm{d}\zeta_{0X_1} \int_{-\infty}^{\nu_2} p(\zeta_{0X_1}, \zeta_{0X_2}) \times \exp\left\{-L_c \int_0^{r_t} [g(\nu_1, h_0, \zeta_{0X_1}, r) + g(\nu_2, h_0, \zeta_{0X_2}, r)]\,\mathrm{d}r\right\} \mathrm{d}\zeta_{0X_2}, \tag{50}$$

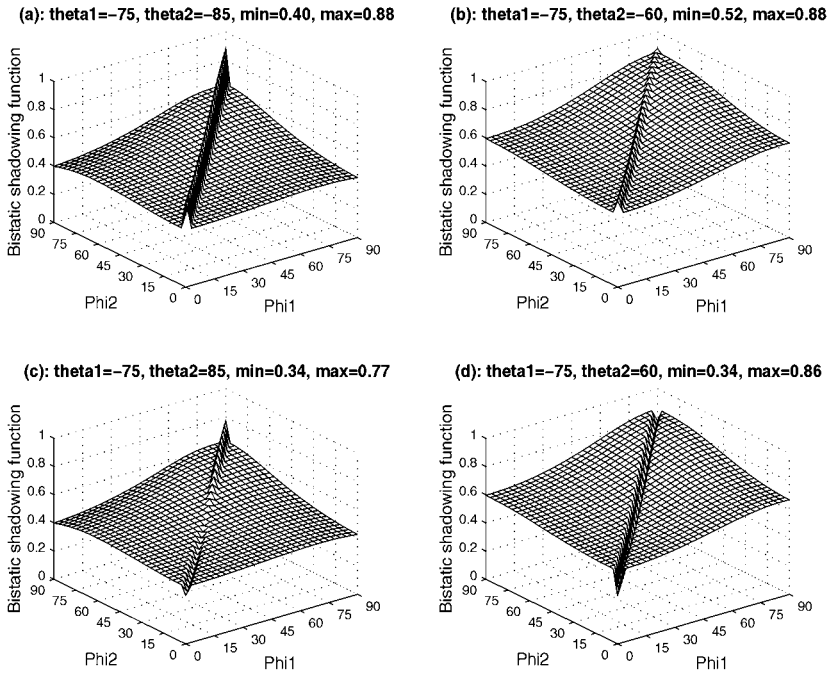

Figure 21. Two-dimensional average bistatic shadowing function versus the azimuthal directions $\{\phi_1, \phi_2\}$ for an uncorrelated Gaussian process with $\{\sigma_x = 0.4, \sigma_y = 0.2\}$, $\theta_2 = \{-85°, -60°, 85°, 60°\}$ and $\theta_1 = -75°$.

where the function $L_c g$ is expressed in table 1 of [26] and integrated numerically. The pdf $p(\zeta_{0X_1}, \zeta_{0X_2})$ is performed from (46) by using the variable transformations $\zeta_{0X_i} = \gamma_{0X_i}/(\sigma_{X_i}\sqrt{2})$

$$p(\zeta_{0X_1}, \zeta_{0X_2}) = \exp\left[-\frac{1}{1-\rho^2}(\zeta_{0X_1}^2 + \zeta_{0X_2}^2 - 2\rho\zeta_{0X_1}\zeta_{0X_2})\right] \Big/ [\sqrt{\pi}(1-\rho^2)^{1/2}]. \tag{51}$$

Therefore, the average bistatic shadowing function is computed from fourfold integrations over $\{\zeta_{0X_1}, \zeta_{0X_2}, r\}$ plus one for the computation of g which required a lot of computer time. Moreover, the numerical solution cannot be computed numerically since two different azimuthal directions of the surface are required which means generating a two-dimensional surface. Thus, only the uncorrelated case is simulated in this paper.

4. Conclusion

In this paper, the monostatic and bistatic shadowing functions from a Gaussian rough stationary surface are investigated. Since, for a one-dimensional surface, the Smith results are better than Wagner's, the Smith model is used as a starting point to calculate the shadowing effect from an anisotropic or two-dimensional surface.

As shown [26], Smith's approach assumes a one-dimensional surface where the correlation between the surface heights and slopes is omitted. To quantify the correlation effect, for monostatic and bistatic configurations, the uncorrelated and correlated average shadowing functions are then compared with an exact numerical solution computed from the generation of the surface Gaussian heights and the algorithm developed by Brokelman and Hagfors [28].

The results show that the correlation can be omitted with a good accuracy. The purpose of the paper is to use the same method for a two-dimensional rough surface.

For a two-dimensional Gaussian surface, we show that the uncorrelated monostatic shadowing function can be obtained from the one defined for a one-dimensional surface, from the substitution of the surface slope rms σ by the surface slope rms $\sigma_X(\phi)$ defined along the azimuthal direction ϕ. Moreover, the correlated case can be performed, from the use of the correlated case where the one-dimensional surface height autocorrelation function is replaced by the one given in polar coordinate functions as $\{R, \phi\}$. R denotes the radial distance between two points on the surface. To compute the numerical solution, the surface height is generated with respect to ϕ from the method exposed in [30]. As in the one-dimensional case, for Gaussian and Lorentzian height correlations and a sea spectrum, the comparison of the different formulations shows the uncorrelated solution overestimates weakly the shadow, whereas the correlated one underpredicts it slightly. This means that the shadowing function does not depend on the autocorrelation function.

For a bistatic configuration, when the transmitter and the receiver are located in the same plane, the comparison of the different approaches yields a similar conclusion. Nevertheless, the deviation between the uncorrelated results and the reference solution is smaller that the one evaluated with the correlated ones. If the transmitter and receiver are in different planes, the correlated solution requires then fourfold integrations and the reference solution cannot be computed since a two-dimensional surface has to be generated. In this paper, only the uncorrelated bistatic statistical function is therefore derived.

In conclusion, as the one-dimensional case, the uncorrelated statistical bistatic shadowing function can be used to a good approximation. This allows us to get a simple statistical shadowing function. Although the simulations presented in this paper assume an infinite observation length, the mathematical formulations take this into account.

Acknowledgment

The authors would like to thank Professor Iosif Fuks for his remarks received by letter on the 'history' of the shadowing function as stated in the introduction.

Appendix. Derivation of the elements of the covariance matrix in polar coordinates

In (27a) and (27b), the functions $\{R_{1x}, R_{1y}, R_{2x}, R_{2y}, R_{2xy}\}$ given by (24a) in Cartesian coordinates (x, y) have to be expressed in polar coordinates $\{R, \phi\}$.

The partial derivatives $\{R_{1x}, R_{1y}\}$ can be defined as

$$\begin{aligned} R_{1x} &= \frac{\partial R_0}{\partial x} = \frac{\partial R_0}{\partial R}\frac{\partial R}{\partial x} + \frac{\partial R_0}{\partial \phi}\frac{\partial \phi}{\partial x} \\ R_{1y} &= \frac{\partial R_0}{\partial y} = \frac{\partial R_0}{\partial R}\frac{\partial R}{\partial y} + \frac{\partial R_0}{\partial \phi}\frac{\partial \phi}{\partial y} \end{aligned} \tag{A.1}$$

where $R_0(x, y)$ is the surface height autocorrelation defined in Cartesian coordinates. We can write

$$\begin{aligned} \frac{\partial R}{\partial x} &= \frac{\partial(\sqrt{x^2+y^2})}{\partial x} = \frac{x}{\sqrt{x^2+y^2}} = \cos\phi \\ \frac{\partial R}{\partial y} &= \frac{\partial(\sqrt{x^2+y^2})}{\partial y} = \frac{y}{\sqrt{x^2+y^2}} = \sin\phi, \end{aligned} \tag{A.2}$$

and

$$\begin{aligned}\frac{\partial\phi}{\partial x} &= \frac{\partial(\text{atan}[y/x])}{\partial x} = -\frac{y}{x^2+y^2} = -\frac{\sin(\phi)}{R}\\ \frac{\partial\phi}{\partial y} &= \frac{\partial(\text{atan}[y/x])}{\partial y} = \frac{x}{x^2+y^2} = \frac{\cos(\phi)}{R}.\end{aligned} \tag{A.3}$$

Substituting (A.2) and (A.3) into (A.1), we have

$$\begin{aligned}R_{1x} &= R_{1R}\cos(\phi) - R_{1\phi}\frac{\sin\phi}{R}\\ R_{1y} &= R_{1R}\sin(\phi) + R_{1\phi}\frac{\cos\phi}{R},\end{aligned} \tag{A.4}$$

where

$$R_{1R} = \frac{\partial R_0}{\partial R}, \qquad \text{and} \qquad R_{1\phi} = \frac{\partial R_0}{\partial\phi}. \tag{A.5}$$

Applying (A.1), the partial derivatives of second order can be written as

$$\begin{aligned}R_{2x} &= \frac{\partial R_{1x}}{\partial x} = \frac{\partial R_{1x}}{\partial R}\frac{\partial R}{\partial x} + \frac{\partial R_{1x}}{\partial\phi}\frac{\partial\phi}{\partial x}\\ R_{2y} &= \frac{\partial R_{1y}}{\partial y} = \frac{\partial R_{1y}}{\partial R}\frac{\partial R}{\partial y} + \frac{\partial R_{1y}}{\partial\phi}\frac{\partial\phi}{\partial y}\\ R_{2xy} &= \frac{\partial R_{1x}}{\partial y} = \frac{\partial R_{1x}}{\partial R}\frac{\partial R}{\partial y} + \frac{\partial R_{1x}}{\partial\phi}\frac{\partial\phi}{\partial y}.\end{aligned} \tag{A.6}$$

We can show that

$$\begin{aligned}\frac{\partial R_{1x}}{\partial R} &= R_{2R}\cos\phi + \left(\frac{R_{1\phi}}{R^2} - \frac{R_{2R\phi}}{R}\right)\sin\phi\\ \frac{\partial R_{1y}}{\partial R} &= R_{2R}\sin\phi - \left(\frac{R_{1\phi}}{R^2} - \frac{R_{2R\phi}}{R}\right)\cos\phi,\end{aligned} \tag{A.7}$$

and

$$\begin{aligned}\frac{\partial R_{1x}}{\partial\phi} &= \left(R_{2R\phi} - \frac{R_{1\phi}}{R}\right)\cos\phi - \left(R_{1R} + \frac{R_{2\phi}}{R}\right)\sin\phi\\ \frac{\partial R_{1y}}{\partial\phi} &= \left(R_{2R\phi} - \frac{R_{1\phi}}{R}\right)\sin\phi + \left(R_{1R} + \frac{R_{2\phi}}{R}\right)\cos\phi,\end{aligned} \tag{A.8}$$

with

$$R_{2R} = \frac{\partial^2 R_0}{\partial R^2} \qquad R_{2\phi} = \frac{\partial^2 R_0}{\partial\phi^2} \qquad R_{2R\phi} = \frac{\partial^2 R_0}{\partial R\,\partial\phi}. \tag{A.9}$$

The substitution of (A.7) and (A.8) into (A.6) yields

$$\begin{aligned}R_{2x} &= \frac{R^2R_{2R}\cos^2(\phi) + \sin^2(\phi)(RR_{1R} + R_{2\phi}) - \sin(2\phi)(RR_{2R\phi} - R_{1\phi})}{R^2}\\ R_{2y} &= \frac{R^2R_{2R}\sin^2(\phi) + \cos^2(\phi)(RR_{1R} + R_{2\phi}) + \sin(2\phi)(RR_{2R\phi} - R_{1\phi})}{R^2}\\ R_{2xy} &= \frac{2\cos(2\phi)(RR_{2R\phi} - R_{1\phi}) + \sin(2\phi)(R^2R_{2R} - RR_{1R} - R_{2\phi})}{2R^2}.\end{aligned} \tag{A.10}$$

From (A.10) and (A.4), we can notice that the partial derivatives $\{R_{1x}, R_{2x}\}$ are obtained from $\{R_{1y}, R_{2y}\}$ defined with respect to y by replacing $\{\sin(\phi), -\cos(\phi)\}$ in $\{\cos(\phi), \sin(\phi)\}$ which is similar to changing ϕ for $\phi + \pi/2$.

The substitution of (A.10) and (A.4) into (27*a*) and (27*b*) gives

$$R_1 = R_{1R} = \frac{\partial R_0}{\partial R}, \qquad \text{and} \qquad R_2 = R_{2R} = \frac{\partial^2 R_0}{\partial R^2}. \tag{A.11}$$

References

[1] Beckmann P and Spizzichino A 1963 *The Scattering of Electromagnetic Waves from Rough Surfaces: Part I. Theory* (London: Pergamon)

[2] Bass F G and Fuks I M 1979 *Wave Scattering from Statistically Rough Surfaces* (Oxford: Pergamon)

[3] Ulaby F T, Moore R K and Fung A K 1982 *Microwave Remote Sensing* vol 2 (London: Addison-Wesley)

[4] Olgilvy J A 1991 *Theory of Wave Scattering from Random Rough Surfaces* (Bristol: Institute of Physics Publishing)

[5] Fung A K 1994 *Microwave Scattering and Emission Models and their Application* (London: Artech House Publishers)

[6] Tsang L and Kong J A 2001 *Scattering of Electromagnetic Waves in Advanced Topics* (New York: Wiley)

[7] Wetzel L B 1990 *Electromagnetic Scattering from the Sea at Low Grazing Angles in Surface Waves and Fluxes* ed G L Geernaert and W L Plant (Dordrecht: Kluwer) ch II pp 109–71

[8] Voronovich A G 1999 *Wave Scattering from Rough Surfaces* 2nd edn (Germany: Springer)

[9] Rice S O 1950 Reflection of electromagnetic waves from slightly rough surfaces *On the Theory of Electromagnetic Wave Conf.* pp 351–78

[10] Thorsos E I and Broschat S L 1989 The validity of the perturbation theory approximation for rough surface scattering using a Gaussian roughness spectrum *J. Acoust. Soc. Am.* **86** 261–77

[11] Bahar E and Lee B S 1996 Radar scatter cross section for two-dimensional random surfaces—full waves solutions and comparisons with experiments *Waves Random Media* **6** 1–23

[12] Bourlier C, Saillard J and Berginc G 2001 Theoretical study on two-dimensional Gaussian rough sea surface emission and reflection in the infrared frequencies with shadowing effect *IEEE Trans. Geosci. Remote Sens.* **39** 379–92

[13] Ginneken B V, Stavidri M and Koenderink J J 1998 Diffuse and specular reflectance from rough surface *Appl. Opt.* **37** 130–9

[14] Yoshimori K, Itoh K and Ichioka Y 1995 Optical characteristics of a wind-roughened water surface: a two-dimensional theory *Appl. Opt.* **34** 6236–47

[15] Sancer M I 1969 Shadow-corrected electromagnetic scattering from a randomly rough surface *IEEE Trans. Antennas Propag.* **17** 577–85

[16] Bourlier C, Berginc G and Saillard J 2001 Theoretical study of the Kirchhoff integral from two-dimensional randomly rough surface with shadowing effect—application on the backscattering coefficient for a perfectly conducting surface *Waves Random Media* **11** 119–47

[17] McCoy J J 1989 Shadowing by randomly rough surface *J. Acoust. Soc. Am.* **86** 1523–9

[18] Bass F G and Fuks I M 1964 Calculation of shadowing for wave scattering from a statistically rough surface *Sov. Radiophys.* **7** 101–12

[19] Kuznetsov P I, Stratonovich V L and Tikhonov V I 1954 The duration of random function overshoots *Sov. Phys.–JETP* **24**

[20] Ricciardi L M and Sato S 1986 On the evaluation of first passage time densities for Gaussian processes *Signal Process.* **11** 339–57

[21] Ricciardi L M and Sato S 1983 A note on first passage time problems for Gaussian processes and varying boundaries *IEEE Trans. Inf. Theory* **29** 454–7

[22] Wagner R J 1967 Shadowing of randomly rough surfaces *J. Acoust. Soc. Am.* **41** 138–47

[23] Smith B G 1967 Lunar surface roughness, shadowing and thermal emission *J. Geophys. Res.* **72** 4059–67

[24] Smith B G 1967 Geometrical shadowing of a random rough surface *IEEE Trans. Antennas Propag.* **15** 668–71

[25] Beckman P 1965 Shadowing of random rough surfaces *IEEE Trans. Antennas Propag.* **13** 384–8

[26] Bourlier C, Berginc G and Saillard J 2002 Monostatic and bistatic statistical shadowing functions from one-dimensional stationary randomly rough surface according to the observation length: part I. Single scattering *Waves Random Media* **12** 145–74

[27] Bourlier C, Berginc G and Saillard J 2002 Monostatic and bistatic statistical shadowing functions from one-dimensional stationary randomly rough surface according to the observation length: part II. Multiple scattering *Waves Random Media* **12** 175–200

[28] Brokelman R A and Hagfors T 1966 Note of the effect of shadowing on the backscattering of waves from a random rough surface *IEEE Trans. Antennas Propag.* **14** 621–9

[29] Bourlier C, Berginc G and Saillard J 2002 One- and two-dimensional shadowing functions for any height and slope stationary uncorrelated surface in the monostatic and bistatic configurations *IEEE Trans. Antennas Propag.* **50** 312–14

[30] Wang H T 1985 Temporal and spatial simulations of random ocean waves *Proc. 4th Offshore Mechanics and Arctic Engineering Conf. (ASME)* vol 1 pp 72–80

[31] Bourlier C, Saillard J and Berginc G 2000 Intrinsic radiation of the sea surface *Progress in Electromagnetic Research* vol 27, ed J A Kong (Cambridge, MA: EMW) pp 185–335
[32] Fung A K and Lee K K 1982 A semi-empirical sea-spectrum model for scattering coefficient estimation *IEEE J. Ocean. Eng.* **7** 166–76
[33] Yoshimori K, Itoh K and Ichioka Y 1995 Optical characteristics of a wind-roughened water surface: a two dimensional theory *Appl. Opt.* **34** 6236–47
[34] Apel J R 1994 An improved model of the ocean surface wave vector spectrum and its effects on radar backscatter *J. Geophys. Res.* C7 **99** 1–21
[35] Elfouhaily T, Chapron B, Katsaros K and Vandemark D 1997 A unified directional spectrum for long and short wind-driven waves *J. Geophys. Res.* C7 **102** 781–96
[36] Cox C and Munk W 1954 Statistics of the sea surface derived from sun glitter *J. Mar. Res.* **13** 198–226
[37] Lemaire D, Sobieski P and Guissard A 1999 Full-range sea surface spectrum in nonfully developed state for scattering calculations *IEEE Trans. Geosci. Remote Sens.* **37** 1038–51